UNIVERSITÀ POLITECNICA DELLE MARCHE

FACOLTÀ DI INGEGNERIA

Corso di Laurea Magistrale in Ingegneria Civile

PROGETTAZIONE E DIMOSTRAZIONE SPERIMENTALE DI METAPALI PER L'ATTENUAZIONE DI ONDE SISMICHE DI TAGLIO

DESIGN AND TABLETOP EXPERIMENTAL DEMONSTRATION OF METAPILES FOR SHEAR SEISMIC WAVES ATTENUATION

Relatore:

Stefano Lenci

Tesi di Laurea di:

Ilaria Nunzi

Correlatori:

Chiara Daraio

Paolo Celli

Anno Accademico 2020/2021

Abstract

La conoscenza approfondita del comportamento dei metamateriali risonanti per la progettazione di una nuova generazione di sistemi di isolamento sismico costituisce un importante argomento di attualità. Nel tempo, sono state introdotte molte strategie di isolamento sismico basate sull'impiego di metamateriali, ma la maggior parte di esse è altamente invasiva e non adatta per il *retrofit*.

La presente tesi dimostra che le onde sismiche possono essere attenuate tramite colonne monodimensionali di risonatori, chiamate "pali di metamateriali" o "metapali", installate attorno a un sito da isolare, piuttosto che proprio sotto quello stesso sito. Il nostro lavoro si incentra sullo studio dell'attenuazione delle onde di taglio che si propagano perpendicolarmente verso la superficie.

La questione chiave è il progetto del design di un metamateriale sismico da impiegare come risonatore in grado di attenuare le onde in un certo intervallo di frequenza. Il progetto del metamateriale risonante è stato sviluppato e analizzato mediante simulazioni numeriche utilizzando il software agli elementi finiti, COMSOL Multiphysics.

I risultati di queste analisi numeriche vengono poi elaborati in MATLAB, da cui si ottengono le loro caratteristiche spettro-spaziali. Le curve di dispersione ed i diagrammi di trasmissione evidenziano la presenza di un *bandgap* risonante a partire da 5.9 kHz, che corrisponde alla frequenza di risonanza di ciascun risonatore nel metamateriale. Questi risultati vengono quindi convalidati testando i risonatori stampati con la stampante 3D utilizzando il setup sperimentale da tavolo sviluppato nel laboratorio della Professoressa *Chiara Daraio*, presso il *California Institute of Technology*. I test sperimentali convalidano le simulazioni numeriche aumentando il livello di accuratezza e confermando la coerenza dei risultati ottenuti. Dopo aver dimostrato che i risonatori progettati sono in grado di attenuare i segnali di onde sismiche di taglio su quello specifico intervallo di frequenza, passiamo allo studio dell'attenuazione delle onde tramite metapali, inserendo colonne di risonatori in una grande lastra acrilica. Questi risultati vengono convalidati anche tramite simulazioni numeriche in COMSOL Multiphysics.

Successivamente, dopo questo studio preliminare in piccola scala, viene fornita una prospettiva futura di applicazione sismica più ampia scalando il modello e studiando il comportamento di diverse configurazioni di risonatori, che agiscono come *tuned mass dampers*, piantati in un semispazio con proprietà simili al suolo, utilizzando il software agli elementi finiti, SAP2000, che consente di implementare più facilmente modelli orientati all'ingegneria civile.

In particolare, effettuiamo un ampio studio parametrico dove analizziamo gli effetti delle caratteristiche dei risonatori e delle diverse configurazioni dei metapali. Questo studio parametrico è molto interessante perché pone le basi per progettare il design ottimale dei metapali. Le mappe ottenute attraverso questo studio possono essere utilizzate per scegliere le caratteristiche e la disposizione dei risonatori in base al livello di attenuazione desiderato, con implicazioni rilevanti nello studio della propagazione e attenuazione delle onde.

Abstract

The implementation of resonant metamaterials for the development of a new generation of seismic isolation systems is a very challenging field for engineering researchers. Even though many metamaterials-based strategies have been introduced in this context, most of them are highly invasive and might not be well suited for retrofitting.

In this thesis we show that seismic waves can be attenuated via buried columns of resonators, called "metamaterial piles" or "metapiles", arranged according to sparse patterns around a site to be isolated, rather than right underneath that same site. Our focus is on shear waves approaching the surface of a half-space from the depth direction, perpendicularly towards the surface itself.

We begin by studying the fundamentals of our idea at a tabletop-scale, where we can compare numerical predictions to experimental results. In particular, we design a resonant metamaterial via numerical simulations using the Finite Element Method software, COMSOL Multiphysics. The results of these analyses are then post-processed in MATLAB, from which we extract their spectro-spatial characteristics of the dynamics of these systems. The dispersion relation curves and the transmissibility diagrams highlight the presence of a bandgap starting at 5.9 kHz, that corresponds to the resonant frequency of each resonator in the metamaterial. These results are then validated by testing 3D printed resonators using a tabletop experimental setup developed within the lab of Professor *Chiara Daraio* at the *California Institute of Technology*. Experimental tests support and validate our numerical simulations. After demonstrating that the proposed resonators work as we expect them to, we go on and validate the idea of wave attenuation via metapiles, by embedding columns of resonators in a large acrylic plate. These results are also validated via numerical simulations in COMSOL Multiphysics.

After this preliminary study at a tabletop-scale, we provide a wider outlook by scaling-up the model and studying the behavior of different arrangements of resonators, that act as tuned mass dampers, planted in a soil-like half-space, this time using the Finite Element Method software, SAP2000, which allows to more easily implement civil engineering-oriented models.

In particular, we perform a wide parametric study where we analyze the effects of the resonators characteristics and their arrangement into metapiles. The maps obtained through this study may be employed to choose resonators characteristics and arrangement based on a desired level of attenuation, with relevant implications in the study of wave propagation and attenuation.

Contents

List of Figures

Acknowledgements

I consider myself exceptionally fortunate to have had the opportunity to work as a Student Researcher at *Caltech*, working with a number of great scientists and meeting wonderful people.

First, I would like to express my greatest appreciation for my co-advisor *Prof. Paolo Celli*, for giving me five months' mentorship and support. I learned a lot from him about doing research and he shared all his knowledge about the topic allowing me to deeply understand the subject. I am very thankful for his remarkable patience in spending hours going through research. He was always willing to help me seeing connections between seemingly unrelated results and make everything fit together.

My deepest gratitude goes to my supervisor at Caltech, *Prof. Chiara Daraio*, for inviting me to join her research group at the *California Institute of Technology*. She allowed me to take part in the Student Research program in order to do research in a very well prepared and professional team of scientists. I am deeply grateful for her guidance and suggestions throughout my research.

I am very thankful to *Prof. Stefano Lenci* that supported my research project from the very beginning allowing me to deeply analyze important aspects and giving interesting further suggestions about the topic.

I would like to thank *Antonio Palermo* and *Andrea Calabrese* for their constructive comments and recommendations during my training.

This master thesis would not have been possible without their contributions and insights.

I am deeply grateful to my family for their support, for standing by my side and believing in me through the hard times, without which this would have been impossible.

Chapter 1
Introduction

1.1 Seismic waves

When an earthquake occurs, rocks at a fault line slip or break, and two sections of Earth's crust physically move relative to one another. The shockwaves of released energy that shake the Earth are called seismic waves, from the Greek "*seismós*" meaning "earthquake". Seismic waves radiate outward from the earthquake through Earth's interior and along its surface.

Seismic waves, that travel through Earth's layers, turn soft deposits, such as clay, into jelly. This phenomenon is called liquefaction. Moreover, they can also be caused by explosions, volcanic eruptions, magma movements, large landslides, man-made explosions that give out low-frequency acoustic energy and many other natural and anthropogenic sources that create ambient vibrations.

The propagation velocity of seismic waves depends on density and elasticity of the medium as well as the type of wave. Earthquakes generate many types of waves with different velocities. The velocity increases with depth through Earth's crust and mantle but drops sharply going from the mantle to the outer core.

Among the many types of seismic waves, it is possible to make a broad distinction between body waves, that travel through the interior of the Earth, and surface waves, that travel across the surface of the Earth.

Body waves arrive prior to the surface waves emitted by an earthquake. These waves are characterized by a higher frequency than surface waves. Seismic body waves can be distinguished in two types of particles motion: P-waves, also known as primary waves or pressure waves, are compressional waves that are longitudinal in nature, and S-waves, also known as secondary waves, shear waves or shaking waves, are transverse waves that travel slower than P-waves.

The first kind of body wave is the P-wave or primary wave. This is the fastest kind of seismic wave, and, consequently, the first to arrive at a seismic station. Moreover, the P-wave can move

through solid rock and fluids, like water or the liquid layers of the Earth. It pushes and pulls the rock, it moves through just like sound waves push and pull air particles. Because of the pushing and pulling they do, P-waves are also known as compressional waves. Subjected to a P-wave, particles move in the same direction of wave propagation, which is the direction that the energy is traveling in.

The second type of body wave is the S-wave or secondary wave. S-waves are slower than P-waves and can only propagate through solids and not through any liquid medium. Because of this property of S-waves, seismologists concluded that the Earth's inner core is a liquid. S-waves move rock particles side to side, with the particle movement being perpendicular to the direction of wave propagation.

Travelling only through the Earth's crust, seismic surface waves are characterized by a lower frequency than body waves. They can be classified as a form of mechanical surface waves: Love waves, Rayleigh waves and Stoneley waves.

The first kind of surface wave is called Love wave, that is the fastest surface wave and moves the ground from side to side. Confined to the surface of the crust, Love waves produce entirely horizontal motion.

The other kind of surface wave is the Rayleigh wave, that rolls along the ground just like a wave rolls across a lake or an ocean. In particular, it moves the ground up and down, and side to side in the same direction of wave propagation.

In the present work, we focus especially on shear waves rather than on longitudinal waves, because during seismic events, even if the S-waves travel at about half the speed of P-waves, they can be much more destructive; consequently, they can inflict the greatest damages to buildings and their contents.

1.2 Seismic Metamaterials

A metamaterial (from the Greek word "*μετά*", meaning "beyond" and the Latin word "*materia*", meaning "matter" or "material") is an architected material engineered to have unprecedented mechanical properties that may not be found in naturally occurring materials. In 1999, *Rodger Walser* (University of Austin, Texas) said: "Metamaterials are macroscopic

composites having man-made, three-dimensional, periodic cellular architecture designed to produce an optimized combination, not available in nature, of two or more responses to specific excitation".

The physical structure of metamaterials is therefore always engineered at a level that is in between the atomic level and the macroscopic level. These structures are often periodic within the "base material" (bulk material) that is used to fabricate the metamaterial.

In other words, metamaterials are materials "beyond" conventional materials; this concept dramatically increased our ability to challenge our physical perception and intuition. Furthermore, the exponential growth in the number of science articles published in this field has shown exceptional promise to provide challenging innovative theoretical concepts and potentials for engineering applications.

Metamaterials are composite systems in which basis elements, that interact, are arranged in well-defined tailored structural geometries. These engineered materials exhibit properties that are not usually found in natural systems and can be exploited in engineering applications [1].

Moreover, their properties depend on their shape rather than on the material they are made of. In other fields, these materials have been designed to bend light [2] and sound [3], transform from soft to stiff, and even dampen seismic waves from earthquakes [4]. But each of these functions requires a specific engineered mechanical structure, making these materials applicable for specific tasks [41].

In the last few years, seismic metamaterials have been employed in the field of tuned-resonators buried in the soil, around buildings foundations or near the soil-structure interface, as local seismic isolators. By exploiting the locally resonant effect of its constituent units, seismic metamaterials are capable of attenuating seismic waves over certain frequency ranges. Resonant metamaterials have been proposed to reflect or redirect elastic waves at different length scales, ranging from thermal vibrations to seismic excitation. Since they are designed to interact with propagating waves, these engineered materials are able to control the propagation of seismic waves. The protection of critical buildings or sensitive areas from earthquakes via metamaterials is of new topical interest [24].

1.2.1 Wave manipulation

The purpose of this thesis can be better understood introducing the problem of waveguiding and transmission [5, 6, 7]. A waveguide is a structure that guides waves. Guided waves can travel at large distances in structures with only little energy loss, enabling the simple harmonic motion of large areas from a single location. These properties make them well suited for the ultrasonic inspection of aircraft, missiles, pressure vessels, pipelines, etc.

A simple form of guided plate waves is the shear horizontal wave, whose particles motion, contained in the horizontal plane, is polarized parallel to the plate surface and perpendicular to the direction of wave propagation. The shear horizontal wave modes are all dispersive. It is known that dispersive longitudinal (axial), flexural, and torsional multi-mode guided waves can simultaneously exist in structures.

Applied mainly in the solid-state physics field, metamaterials opened up a new range of possibilities to control and shape the propagation of waves.

In this context, a waveguide can be obtained from a metamaterial by removing some of its periodically arranged resonators, as to create a path of defects, and by exciting the system at the frequency of the resonant bandgap.

If the path is wider than the wavelength, waves will travel only along the path, while they will be attenuated outside of it; if the path is narrower than the wavelength, waves cannot be transmitted along that path and are attenuated despite the presence of defects.

Similarly, we want to demonstrate that sparse metapiles can attenuate waves as long as their distance is small enough with respect to the wavelength, so that the wave barely perceives the absence of resonators.

1.2.2 Wave propagation and Bloch's theorem

In this section, aspects related to wave propagation are introduced. As mentioned above, metamaterials are often obtained by the repetition of a single unit cell. Periodic structures are employed because of their outstanding static properties. However, the properties that they manifest when subjected to dynamic loads are even more unique. Periodic structures can be designed to suppress the propagation of seismic waves over certain frequency range. The region

in which there is waves attenuation is called bandgap and its extent can be determined following an analysis based on the Floquet-Bloch theorem.

In particular, the wave propagation in any two-dimensional periodic structure having infinite dimensions can be studied by analyzing a single unit cell [8]. This can be achieved by using concepts and procedures coming from solid state physics, like Bloch's theorem, in conjunction with a finite elements scheme; this de facto amounts to applying wave-like periodic boundary conditions. Please note that this section is heavily inspired by the work of *P. Celli* [8]; we replicate here so that the reader can better understand this important tool used in this thesis.

Considering a harmonic wave response, the displacement of a generic point P of a reference unit cell that undergoes a wave propagating with frequency ω can be written as:

$$w(r_P) = w_{P_0} e^{i(\omega t - k \cdot r_P)} \text{ (Eq. 1.1)}$$

where w_{P_0} is a vector of amplitudes and k is the wave vector, whose modulus is the wave number $k = |k| = 2\pi/\lambda$, reciprocal of the wavelength λ and whose dimension is $[length]^{-1}$. According to Eq. 1.1, the displacement of the point corresponding to P at location $\rho_P(n_1, n_2)$ can be written as:

$$w(\rho_P) = w_{P_0} e^{i(\omega t - k \cdot \rho_P)} \text{ (Eq. 1.2)}$$

It is now possible to manipulate Eq. 1.2 by substituting the expression for ρ_P and by projecting the wave vector along one of the vector bases. Then, k is decomposed on the reciprocal lattice vector basis, as shown in Eq. 1.3:

$$k = \xi_1 b_1 + \xi_2 b_2 \text{ (Eq. 1.3)}$$

Since k, b_1 and b_2 have dimension of $[length]^{-1}$, it follows that ξ_1 and ξ_2 are nondimensional. From Eq. 1.3, ξ_1 and ξ_2 are components of the vector k on the reciprocal lattice vector basis B. Moreover, they are also the projections of k along the directions of vectors e_1 and e_2, since:

$$e_1 \cdot k = \xi_1 b_1 \cdot e_1 + \xi_2 b_2 \cdot e_1 = \xi_1 \text{ (Eq. 1.4)}$$

$$e_2 \cdot k = \xi_1 b_1 \cdot e_2 + \xi_2 b_2 \cdot e_2 = \xi_2 \text{ (Eq. 1.5)}$$

Therefore, the choice of the reciprocal lattice as vector basis to decompose k leads to important simplifications and this is one of the reasons why this basis has been introduced. The position of any point P of a lattice with respect to the origin of the direct lattice reference frame can be

expressed as a function of the position of the corresponding point that belongs to the reference cell:

$$\rho_P(n_1, n_2) = r_P(0,0) + n_1 e_1 + n_2 e_2 \text{ (Eq. 1.6)}$$

Substituting Eq. 1.6 and Eq. 1.3 into Eq. 1.2, the following expression is obtained:

$$w(\rho_P) = w_{P_0} e^{i(\omega t - (\xi_1 b_1 + \xi_2 b_2)\cdot(r_P + n_1 e_1 + n_2 e_2))} \text{ (Eq. 1.7)}$$

By developing the dot product in the exponent and by recalling that $b_1 \cdot r_P = \eta_1$ and $b_2 \cdot r_P = \eta_2$, it can be written that:

$$w(\rho_P) = w_{P_0} e^{i(\omega t - \xi_1 \eta_1 - \xi_2 \eta_2)} e^{-i(\xi_1 n_1 + \xi_2 n_2)} = w(r_P) e^{-i(\xi_1 n_1 + \xi_2 n_2)} \quad \text{(Eq. 1.8)}$$

This equation can be seen as an expression of the Bloch's theorem and it can be also generalized as:

$$w(\rho_P(n_1 + 1, n_2 + 1), t) = w(\rho_P(n_1, n_2), t) e^{-i(\xi_1 n_1 + \xi_2 n_2)} \text{ (Eq. 1.9)}$$

This last expression highlights the meaning of Bloch's theorem, which states that the solution of the wave propagation problem is periodic in the lattice. The application of Bloch's theorem to the unit cell allows to derive all the characteristics of the wave propagation behavior in periodic structures.

Moreover, it is possible to reduce the study of an infinite array of unit cells to the analysis of a single unit cell, by applying the Floquet-Bloch quasiperiodicity conditions [9]. Hence, a frequency dispersion analysis can be carried out and the bandgaps of the unit cell can be determined. Coupling this technique with a FEM description of the unit cell allows extending this approach to cells with arbitrary geometry and internal complexity.

1.3 Previous investigations

Wave propagation in periodic structures in its primal form dates back in the Eighteenth and Nineteenth centuries, with the work on spring-mass chains by *Newton, Cauchy, Baden-Powell* and *Kelvin*. A complete chronology of initial discoveries about this topic can be found in the classic work of *L. Brillouin* (1946) [10], who deals with a wide variety of problems, ranging from wave propagation in periodic structures to wave propagation in electric lines. In particular,

he shows how these structures can be studied by taking advantage of their spatial periodicity, using Floquet's principle and its generalization to the three-dimensional case, i.e. Bloch's theorem, that allows to investigate the behavior of the whole lattice by studying a single unit cell of it. Periodic structures act as filters as a result of the *impedance mismatch*, i.e. the difference in specific impedance caused by the alternation of different media along the wavepaths. This mismatch causes destructive wave interference at specific frequencies and results in the so-called band-stop behavior [8].

The first realization of a metamaterial demonstrated the ability to control electromagnetic waves below the materials' fundamental diffraction limit, as done by *J. Pendry et al.* (2000) [11] and *R. A. Shelby et al.* (2001) [12]. More recently, researchers extended their interests in the study of materials able to control elastic waves, targeting ultrasonic applications in acoustic imaging (*Z. Liu et al.* (2000) [13]) and acoustic cloaking devices (*N. Stenger et al.* (2012) [14] and *L. Zigoneanu et al.* (2014) [15]).

Both elastic and acoustic metamaterials made from locally resonant arrays can exhibit bandgaps at wavelengths much larger than the lattice size for various applications spanning from low-frequency vibration and sound attenuation to wave guiding and filtering in mechanical and electromechanical devices. For an effective use of such locally resonant metamaterial concepts in finite structures, it is required to bridge the gap between the lattice dispersion characteristics and modal behavior of the host structure with its resonators [16]. *C. Sugino et al.* (2016) develop a novel argument for bandgap formation in finite-length elastic metamaterial beams, relying on the modal analysis and the assumption of infinitely many resonators, showing that the dual problem to wave propagation through an infinite periodic beam is the modal analysis of a finite beam with an infinite number of resonators. By using a simple formula that depends only on the resonator natural frequency and total mass ratio, it is possible to place the bandgap in a desired frequency range [16].

The recent development of metamaterial science opens a new direction to control seismic waves. Metamaterials have been proposed as shield in order to protect critical infrastructures from different types of seismic waves [4, 33, 40]. In other words, if locally resonant structures are periodically placed in a matrix material, the resulting metamaterial forms a phononic lattice that creates a stop band able to forbid elastic wave propagation within a selected bandgap frequency range. In particular, conventional phononic lattice structures need huge unit cells for low-frequency vibration shielding, while locally resonant metamaterials can rely on lattice

constants much smaller than the longitudinal wavelengths of propagating waves (*V. La Salandra et al.* (2017) [9]).

When it comes to seismic metamaterials, *Cheng* and *Shi* (2018) studied a periodic foundation composed by a reinforced concrete matrix and steel masses that are connected to the matrix with rubber layers. Hence, demonstrating the effectiveness of their isolation system, they applied it to a nuclear power plant [17]. In another project, *Casablanca et al.* (2018) proposed a foundation composed by concrete plates with embedded cylindrical steel resonators [18].

Therefore, several studies present applications of such materials on foundations. Depending on the different kind of seismic waves they are able to attenuate, they can be distinguished in two main categories, metabarriers and metafoundations (*Colombi et al.* (2020) [19]).

Metabarriers, also known as metasurfaces, comprehend arrays of resonators settled above or right below the surface of a half-space domain. They are employed to attenuate seismic surface waves generated by either natural or man-induced events and they are located around a sensitive building to be protected [21-24, 42-44]. Their attenuation capacity relies primarily on a surface-to-bulk mode conversion produced by the array of resonators. The energy released by surface waves is not allowed to propagate in that form due to the presence of surface wave bandgaps and is therefore converted into non-surface modes.

Metafoundations are foundations featuring metamaterial inspired designs installed underneath a target structure and capable of attenuating waves approaching this structure from the depth direction [9, 15, 45].

These systems can be realized in two ways. The first one consists in incorporating resonant units within the structural elements that compose foundations, such as concrete slabs or walls, as shown in the work of *V. La Salandra et al.* (2017) [9], where they have investigated 3D structured foundations with effective attenuation zones conceived as vibration isolation systems for storage tanks. Additionally, they can be performed by completely altering the foundation design and introducing resonating entities, as done by *S. J. Mitchell et al.* (2014) [20]. In their work, seismic metastructures consist of arrays of cylindrical tubes containing a resonator suspended by soft bearings. To obtain broadband attenuation characteristics, each resonator in the array is designed to exhibit a different eigenfrequency. Furthermore, *Brùlé et al.* (2014) studied the effect of a periodic arrangement of pile foundations in soft soil as if it is a giant soil-phononic crystal with bandgap at 50 Hz [4].

In all metamaterials-based strategies, the wave attenuation performance depends on the number of resonators involved (up until a certain number of resonators, above which the attenuation performance plateaus). When properly engineered, the seismic metamaterial is able to isolate ground vibrations and seismic waves within a specific range of frequencies referred to as bandgaps.

Scientists have thought about using an array of trees, i.e. a forest, acting as sub-wavelength locally resonant metamaterials for Rayleigh surface waves, as demonstrated in the work of *A. Colombi et al.* (2016) [21]. The longitudinal resonances of trees coupled with the vertical compontent of the Rayleigh wave, attenuate the surface ground motion by redirecting part of the elastic energy into the bulk. Further analysis, investigated in "*The METAFORET Project*" (2018) by *P. Roux et al.*, have shown that a pine tree forest behaves as sub-wavelength coupled resonators for seismic surface waves, showing the presence of frequency bandgaps for Rayleigh waves featuring compressional and flexural resonances of the trees [22, 23].

A. Palermo et al. (2016) proposed a soil-embedded surface seismic metabarrier for Rayleigh waves mitigation, in which an array of resonators is employed to redirect surface waves into the bulk and to attenuate the ground motion within the 1-10 Hz range [24].

1.4 Aims of present study

The aim of this master thesis is to investigate the behavior of a metamaterial featuring a minimal number of resonators, and to explore its application to seismic wave attenuation.

To realize this, we propose a strategy that differs from classical metamaterials-based approaches by introducing the concept of "metapiles", defined as one-dimensional arrays of resonators placed near the half-space surface and located around, rather than underneath, a target location to be shielded.

A key issue of the present work is trying to minimize the number of resonators employed in a metabarrier or metafoundation, since this aspect is extremely important for the realization of cost-effective metamaterial-based devices [19].

This work is especially motivated by the fact that most of the studies on seismic metamaterials have been theoretical and numerical, and focused on shielding surface waves.

We focus especially on the study of the attenuation of shear waves that are approaching the surface of the half-space from depth, since seismic events typically generate shear waves that are larger than compression waves. Moreover, shear waves are also responsible for ground shaking, whose consequences can inflict the most damage to sensitive buildings that are not designed to withstand them. The control of this type of waves is an essential paradigm for seismic protection of structures via metamaterials.

Since the metafoundation represents an innovative foundation, which relies on the concept of "local resonance", its resonating units require to be settled directly below the building or the area that we want to protect. Thus, they cannot be easily applied to existing structures after their construction, without the possibility to retrofit them once installed.

We demonstrate that sparse arrangements of engineered vertical pillars of resonating metamaterials allow to significantly attenuate shear waves approaching from the depth direction the target location of a reference point, where a critical structure is located.

A better explanation of this idea is illustrated in the schematic of Figure 1.1 (a).

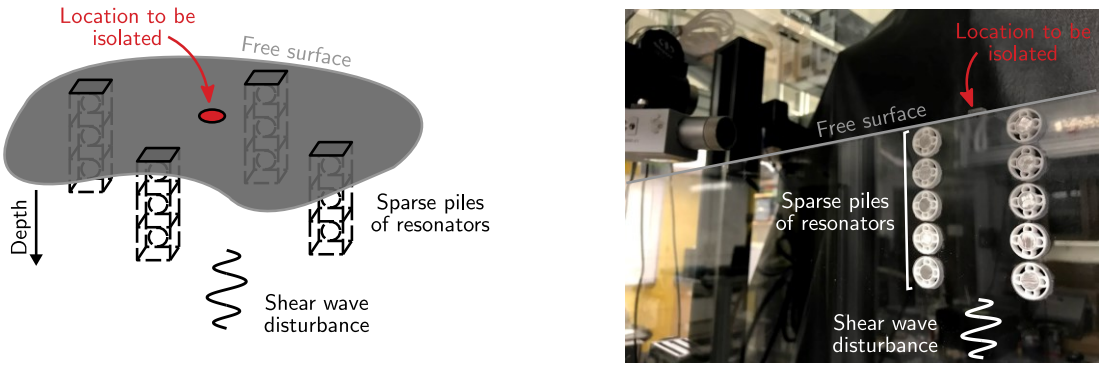

Figure 1. 1: The concept of metapiles. (a) Sketch that illustrates the proposed idea of attenuating shear waves with sparse metapiles. (b) Tabletop-scale experimental setup for proof-of-concept.

The rest of the work is organized as follows. Chapter 2 introduces the reader to the resonators design together with the numerical analysis of the unit cell. The Finite Element model adopted for the numerical analysis of the array of resonators is explained, describing the experimental setup used to validate this idea using 3D printed resonators. Chapter 3 reports the experiment on the acrylic plate by embedded two metapiles of resonators, validating the physics at a tabletop-scale, as shown in Figure 1.1 (b). In section 4, we extend this idea to wave attenuation in an elastic half-space representing a soil medium. Then, virtual simulations outcomes are compared with these experimental results, focusing on the most minimalistic case. Finally, in the last chapter, considerations and future outlook are discussed.

Chapter 2
Resonator design, fabrication, and testing

2.1 Background

The first biggest challenge of my thesis is to design a resonator that can be suitable for our purpose. Prior to this work, others in the Daraio group at Caltech attempted to design polymer-metal composite resonators to be used to test at a tabletop-scale ideas that could be potentially applicable to attenuate seismic waves. Hence, their goal was to design a resonator that would work well and to create an experimental platform to demonstrate a bunch of different physical effects related to seismic waves attenuation.

However, the resonators design that they proposed has a very simple geometry, as shown in Figure 2.1. They are composed by an inner cylinder of steel surrounded by a silicon rubber ring, but there were some implementation difficulties. Since the silicon rubber is a soft elastomer, this design is known to feature a large damping [25]; consequently, the frequency of resonance is low, about 1 kHz. The problem of working at 1 kHz was that the wavelength in the acrylic plate where the resonators were supposed to be embedded was bigger than the size of the plate itself, so that they could not see multiple wavelengths in a tabletop experiment. Further imprecisions were due to the fact that it was difficult to center the cylinder of steel in the hole, since the silicon rubber was too soft.

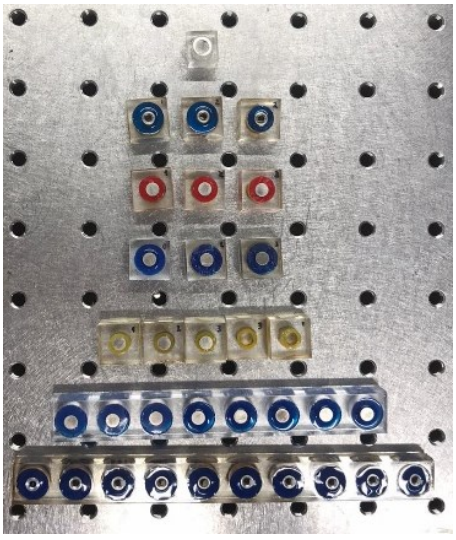

Figure 2. 1: The resonators implemented by *Paolo Celli* and *Antonio Palermo*.

In light of these considerations, our purpose is to design a composite resonator that resonates at higher frequency, between 6-7 kHz, and capable of attenuating shear waves once it is embedded into an acrylic plate.

2.2 Design of the resonator

A resonator can be defined as a mass-spring-dashpot system; if it is attached to another vibrating medium, it can also be seen as a tuned mass damper, also known as a harmonic absorber or seismic damper.

The concept of tuned mass damper (TMD) dates back to year 1909, when *Frahm* invented a vibration control device called dynamic vibration absorber. Few years later, in 1928 *Ormondroyd* and *Den Hartog* improved the performance of the TMD by introducing damping in *Frahm*'s absorber.

Basically, a TMD is a device mounted on one or more damped springs in structures to reduce the amplitude of mechanical vibrations. Tuned mass dampers are used to reduce the maximum vibration amplitude of a system with a comparatively lightweight component so that the worst-case vibrations are less intense.

Our purpose is to design a resonator, whose components act like a spring, a mass and a dashpot.

2.2.1 Considerations on geometry

To better frame the design issue, we need to focus on the following expression:

$$\omega_0 \propto \sqrt{\frac{stiffness}{inertia}}$$

This explains how stiffness and mass influence the eigenfrequency (natural frequency), ω_0, of the mass-spring-dashpot system. Variations in the mass of the resonator and/or in the stiffness of the suspending springs allow varying the resonator characteristic eigenfrequency. This expression enables to understand how to modify the geometry of the resonator and how to choose the right materials, for this specific case.

The resonant frequency of the resonator can be tuned by changing one or more of these three parameters. In other words, if the frequency of resonance that we want for our resonator is around 6-7 kHz, we can increase or decrease its stiffness and its inertia, i.e. modifying the geometry, moving the circular springs around, changing their diameter or the outer diameter of the resonator or the dimension of the inner mass.

How do we design the resonator?

First, we consider a unit cell, an acrylic plastic block whose dimensions are: 60 mm by 20 mm, 6.35 mm thick, with a hole in the middle, in which the resonator, made of a 3D printed polyamide material, is located. In the center of the resonator, we place an inner steel mass.

Hence, we tried different resonators geometries, few of them are shown in Figure 2.2, and we implement all of them on the Finite Element Method software, COMSOL Multiphysics.

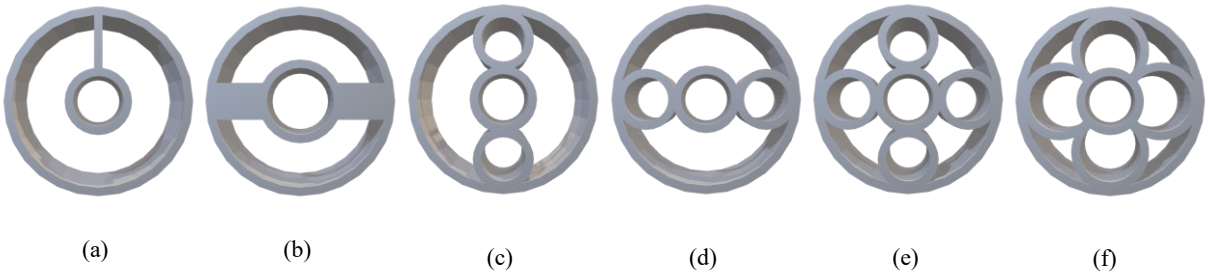

Figure 2. 2: Sketches of the different geometries proposed.

The external diameter of these resonator designs is 18 mm, and the resonating heavy mass takes place in the inner circle. The thickness of the polyamide walls is 0.8 mm.

The first geometry depicted in Figure 2.2 (a) can be seen as a pendulum, where the heavy mass whose diameter is 4.8 mm, is suspended by a rod of 1.5 mm length from the resonator wall. This resonator design gives a wide damping and a low frequency of resonance since the pendulum can oscillate freely.

The concept of the geometry (b) is similar to the previous one, but in this case, the inner mass is heavier because its diameter is 6.35 mm. Thus, it is hung with two rods, whose dimensions are 1.3 mm length and 3.5 mm thick.

Therefore, this design is too stiff for our purpose, so we tried to design circles around, instead of rods, that act like springs for the resonating mass.

In the following two geometries, (c) and (d), the inner mass is connected to the external wall by two circles, whose diameter is 5.8 mm. These circles are located in different positions: in the first case, the circles are located in a vertical way along y axis, while in the second one, they are horizontally aligned along x axis. The behavior of these two designs presents opposite characteristics that depend on the position of the two circles. In fact, the geometry with circles along the vertical shows a little bandgap for shear waves, while the one with the circles in horizontal presents a bandgap for longitudinal waves.

To overcome any doubts related to this behavior, we need to find a compromise between all of them, so we prefer to focus on a symmetric resonator design. Hence, we propose the design (e) with four circles around the inner mass, making the resonator design symmetric with respect to each axis.

However, we try another design (f) that presents four arches around the inner circle, but it works worse than the previous one, so we will not consider it at all.

So far, only the design (e) seems to be suitable for our purpose. In fact, we decide to test this geometry both numerically in COMSOL Multiphysics, as done for all the others, and then, also experimentally.

2.2.2 Materials

The mechanical properties of the acrylic plastic (PMMA) are the following: Young's Modulus E = 5.5 GPa, Poisson's ratio $\nu = 0.35$ and density $\rho = 1190$ kg/m^3. The resonating inner mass is made of "Grade 304 Stainless Steel", whose nominal properties are: Young's Modulus E = 193 GPa, Poisson's ratio $\nu = 0.27$ and density $\rho = 8000$ kg/m^3.

For the resonator spring, we need to choose a 3D printing material via selective laser sintering. In order to understand which material is best, we compute in COMSOL Multiphysics and test the same resonator geometry (Figure 2.2 (e)) considering two different polyamide materials (Appendix - A).

The first one is called "White Natural Versatile Plastic" (PA2200), whose properties are: Young's Modulus E = 1.7 GPa, Poisson's ratio $\nu = 0.34$ and density $\rho = 930$ kg/m^3.

The other material's name is "DM8530-Grey60", whose properties are: Young's Modulus E = 1.3 GPa, Poisson's ratio ν = 0.38 and density ρ = 1150 kg/m^3.

2.2.3 Implementation in COMSOL

The Finite Element Method (FEM) software employed to numerically analyze the resonators design is COMSOL Multiphysics.

First of all, the study starts with a detailed eigenfrequency analysis of the metamaterial, that is the unit cell containing the resonator. Floquet-Bloch periodic boundary conditions are applied to the long edges of the unit cell, while free boundary conditions on the short edges. As previously said, Floquet-Bloch boundary conditions simulate the response of an infinite 1D array of resonators made by replicating this unit cell to waves traveling along its length.

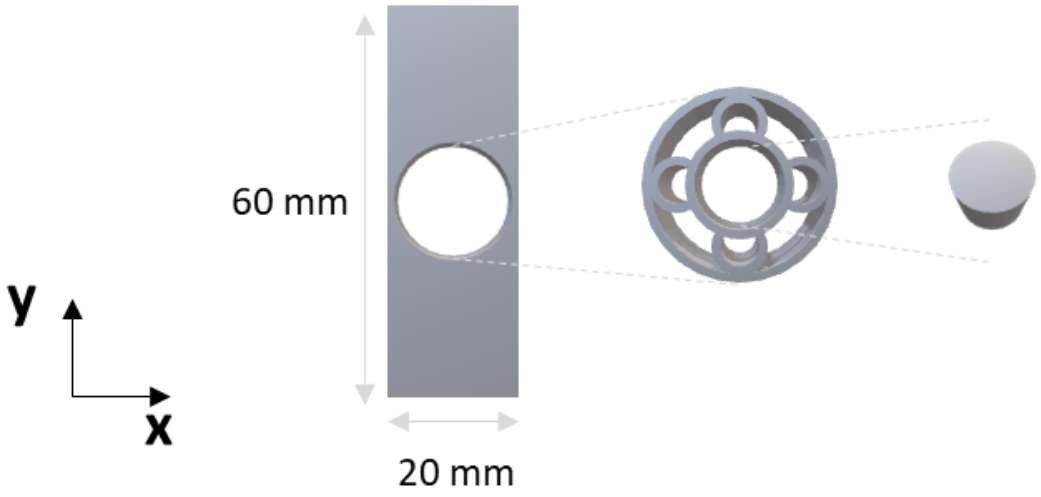

Figure 2. 3: Sketch of the unit cell.

These waves are those that propagate along x, in a direction that is perpendicular to the h dimension of the strip, as shown in the sketch of Figure 2.3. This choice is motivated by the fact that the h dimension of 60 mm is significantly larger than the dimension of the short edge, that is 20 mm. Thus, in this way we simulate wave speeds that are comparable to those we expect when the resonators are embedded in a large acrylic plate and not in the neighboring of the plate's boundaries.

In the eigenfrequency analysis, such elastic waves can be represented by means of dispersion relation curves. Generally, a system can be described by distributed mass and stiffness. There are infinite degrees of freedom for a continuous system, which results in infinite modes. For a finite frequency range, there is a finite number of modes that can be analyzed individually using modal decomposition. The motion of such continuous systems is described by partial differential equations from force/acceleration and force/deformation relations. The solution to such equations can be visualized using two approaches: eigenmodes and wave representation, also known as wave modes. In modeling the dynamics of a large system at higher frequencies using the Finite Element Method software, to capture its behavior, the wavelength must be discretized with a sufficient number of elements [47]. We tackle this issue using wave modes or representing the system as guided waves, since the waves travel long distances before they decay.

Here, a parametric sweep for the wavenumber k along x direction is performed. This allows to change the parameter values, k_x, through a specified range, instead of manually changing these property values and resolving each time.

In this specific case, the range chosen goes from 0 to π/a, searching for eigenfrequencies around 1 Hz, while the desired number of eigenfrequencies is 15. This model provides accurate results only with very fine tetrahedral meshing.

2.2.4 Numerical results of the designs proposed

After analyzing carefully all the resonator designs proposed, we implement those geometries of resonators (Figure 2.2) on COMSOL Multiphysics. The study of the different models leads us to develop the most suited design for the following experiments on seismic waves.

In this section, all the results obtained from the eigenfrequency analyses, computed in COMSOL and post-processed in a MATLAB code, are illustrated. In this step, we consider the resonators made of polyamide PA2200.

In particular, the derived volume average values extracted in the form of tables from these models are concerned the displacement fields along x and y, and the total displacement. Then, exporting these values from COMSOL to a MATLAB code, we obtained the band diagrams illustrated in the following pictures for all the designs.

For each design depicted in Figure 2.2, the dispersion relation curves computed with the results of the eigenfrequency analysis are reported.

The dispersion relation curves, which are frequency [kHz] versus wavenumber [1/m], allow to identify specific modes of wave propagation. In particular, each of these wave modes curves is pointed out by a series of circular markers, that are automatically color-coded depending on the characteristics of the corresponding mode shape. Hence, when the displacement along x over the total displacement is bigger than a chosen index, the circular markers corresponding to the longitudinal wave mode are color-coded. Contrarily, when the displacement along y over the total displacement is bigger than a chosen index, the circular markers corresponding to the shear wave mode are color-coded.

In the following diagrams, the red markers represent a shear mode of wave propagation, while all the other points correspond to longitudinal, torsional or mixed modes.

Since the mode we are mostly interested in is the shear mode, we carefully study the trend of the shear mode.

In the dispersion relation diagram of the first design (Figure 2.2 (a)), in which the resonator is similar to a pendulum, we notice that the bandgap is very narrow, starting at a frequency of 6.6 kHz, while the other branch, that define the width of the bandgap, is at 6.7 kHz (Figure 2.4).

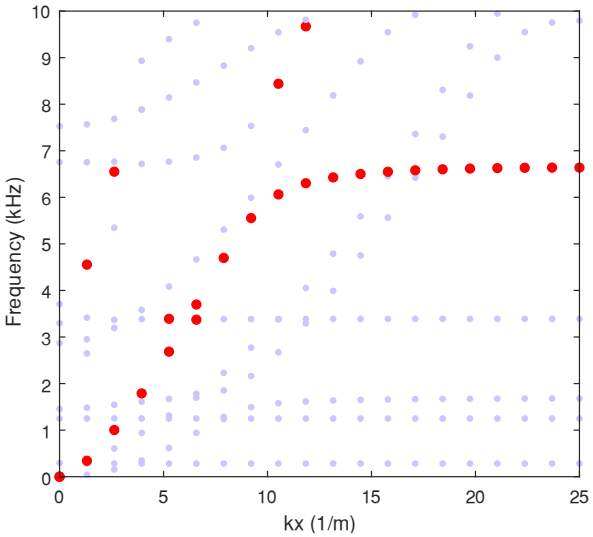

Figure 2. 4: Dispersion relation for the design corresponding to Figure 2.2 (a).

In Figure 2.5, the dispersion relation curve of the design (b) shows a bandgap that is still very narrow, that goes from 6.1 kHz to 7.2 kHz.

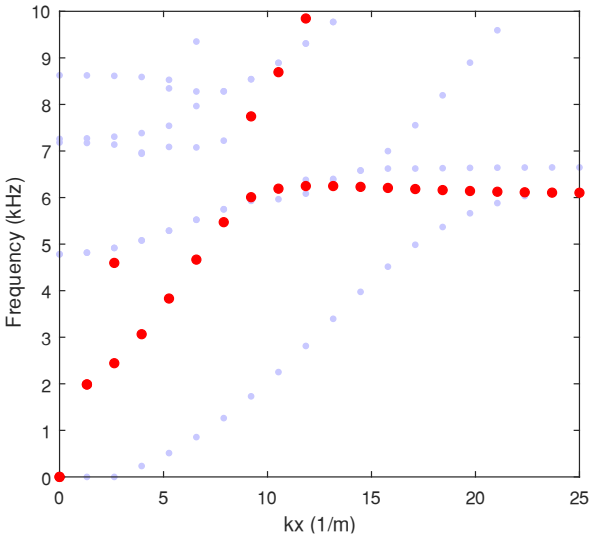

Figure 2. 5: Dispersion relation for the design corresponding to Figure 2.2 (b).

In the band diagram of the design (c), shown in Figure 2.6, the branch of the shear mode flattens at a frequency of 5.9 kHz, that is where the bandgap is supposed to start, and it ends at about 6.3 kHz.

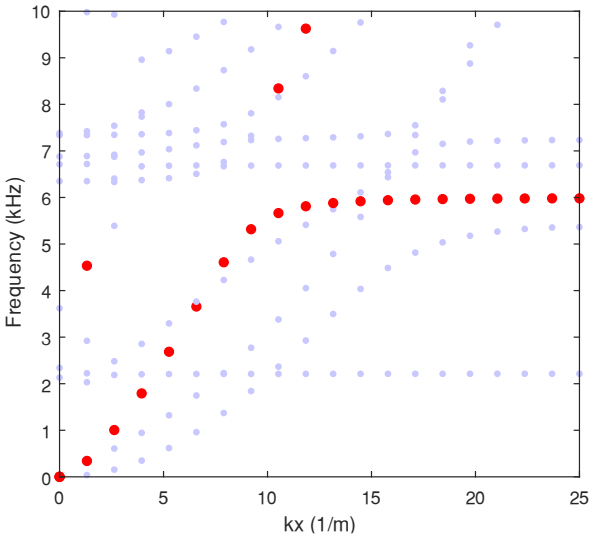

Figure 2. 6: Dispersion relation for the design corresponding to Figure 2.2 (c).

As shown in the following Figure 2.7, there is no bandgap for the resonator design (d).

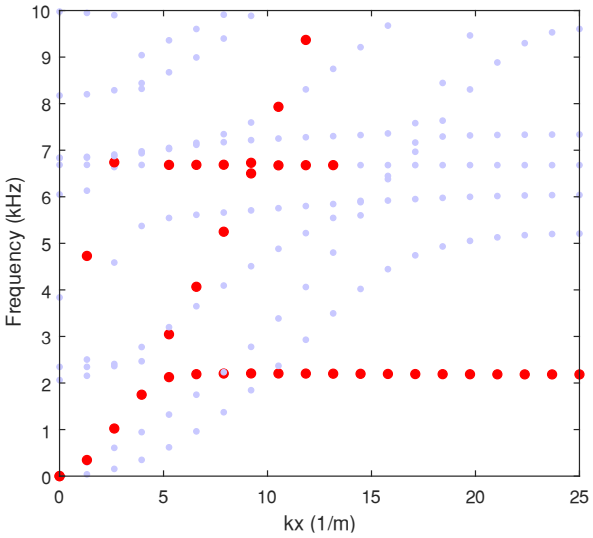

Figure 2. 7: Dispersion relation for the design corresponding to Figure 2.2 (d).

The next two graphics show the dispersion relation curves for the shear wave mode, considering the design (e) with the four circles around the resonating mass. In particular, we consider the same resonator design, but in the first case the dispersion relation, plotted in Figure 2.8, refers to a resonator made of polyamide called “White Natural Versatile Plastic” (PA2200), while in the second case the dispersion relation illustrated in Figure 2.9 belongs to a resonator made of polyamide called “Grey 60” (DM8530).

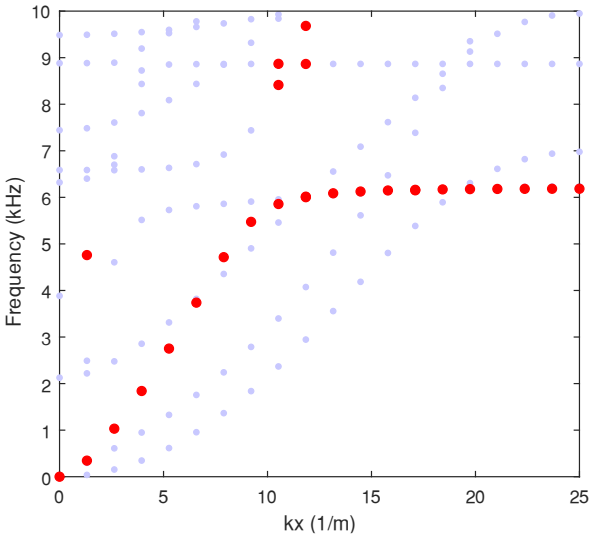

Figure 2. 8: Dispersion relation for the design corresponding to Figure 2.2 (e) made of PA2200.

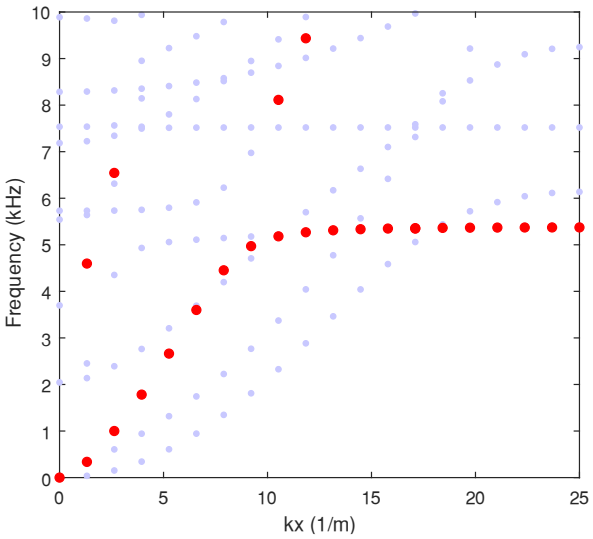

Figure 2. 9: Dispersion relation for the design corresponding to Figure 2.2 (e) made of DM8530.

The two red dotted curves in both cases show a bandgap that starts in the first case at 6.2 kHz, while in the second one at 5.3 kHz. In both cases, the resonant bandgap is caused by resonant dynamics of the polymer-steel resonator and its width is about 0.4 kHz.

For the resonator spring material, we prefer working considering the white polyamide (PA2200), with a Young's Modulus of 1.7 GPa, that is stiffer than the grey polyamide (DM8530), whose Young's Modulus is 1.3 GPa.

Another motivation that enhances this choice is due to the fact that, besides the width of the gap is almost the same for the two bandgaps, the gap relative to the white resonator is located above, closer to the frequency range we are interested in.

2.2.5 The resonator of choice

In light of these results coming from the numerical simulations in COMSOL, we decide to focus on this last design (Figure 2.2 (e)). Therefore, we continue working on this design, improving it, modifying its geometry, in order to gain better results, that would be more suitable for the attenuation of shear waves in a frequency range between 6-7 kHz.

After many other attempts, in the end, the design that we choose for the present study is the circular resonator depicted in Figure 2.10.

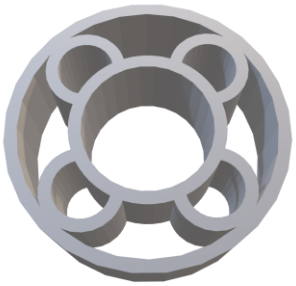

Figure 2. 10: 3D model of the resonator design chosen for this work.

However, the resonator is a circular polyamide casing with four circular springs around an inner circle where the heavy metallic mass is located. The four circles, that surround the circle in the middle, make the resonator symmetric to each axis.

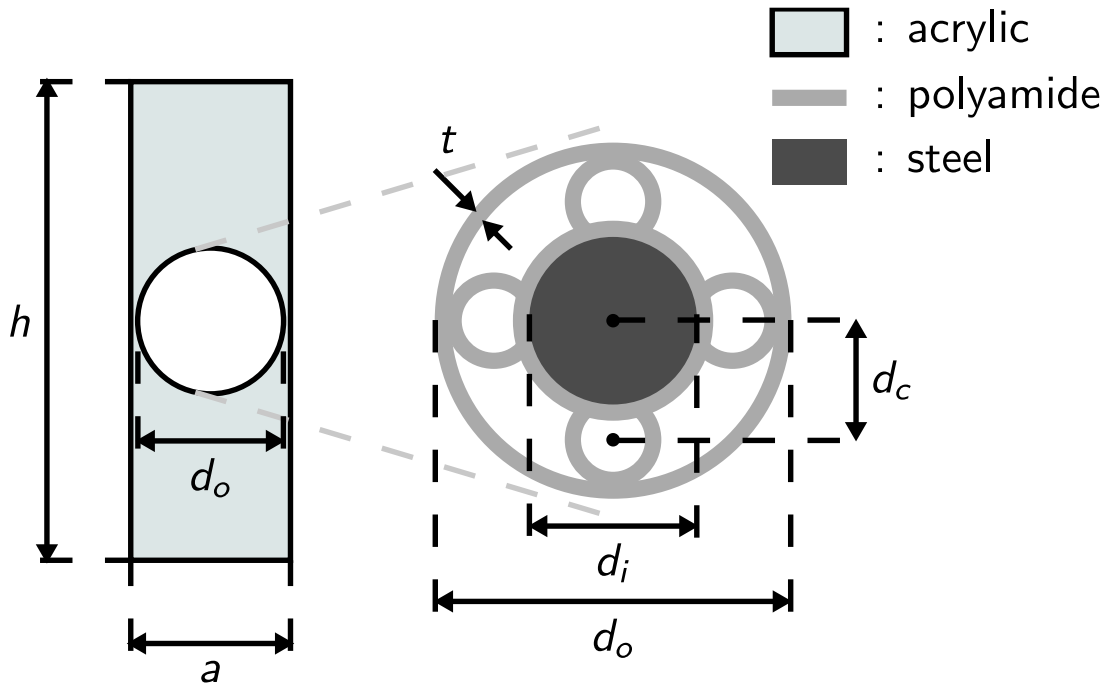

Figure 2. 11: 3D printed resonator design. Unit cell for the one-dimensional tests with its relevant dimensions.

In order to numerically test this design in COMSOL Multiphysics, we implement a unit cell of acrylic plastic, whose dimensions are height h = 60 mm, width a = 20 mm and out-of-plane thickness b = 6.35 mm, as described in Figure 2.11.

Basically, it is a strip with a hole of diameter d_0 = 18 mm in the middle, where the resonator takes place. The thickness of the polyamide walls is t = 0.85 mm, the total diameter of the resonator is d_0 = 18 mm, and the diameter of the heavy mass is d_i = 8.4 mm. The diameter of the four circles around is 5.2 mm. The distance between the center of the heavy mass and the center of one of the circular springs is d_c = 5.7 mm.

To sum up, this is the resonator geometry that is well-suited for the present study on the attenuation behavior. Thus, we focus on this design that is modeled and computed in COMSOL Multiphysics for the first study step: the eigenfrequency analysis.

2.2.6 Numerical results of the unit cell

As carefully explained before, from the eigenfrequency analysis of the unit cell with the resonator embedded, the derived volume average values are extracted. In particular, the output data obtained from this analysis are the values of the displacement fields along x and y, and the total displacement. Then, elaborating these tables extracted from COMSOL Multiphysics, and then exported to a MATLAB code, we obtain the band diagram illustrated in Figure 2.12.

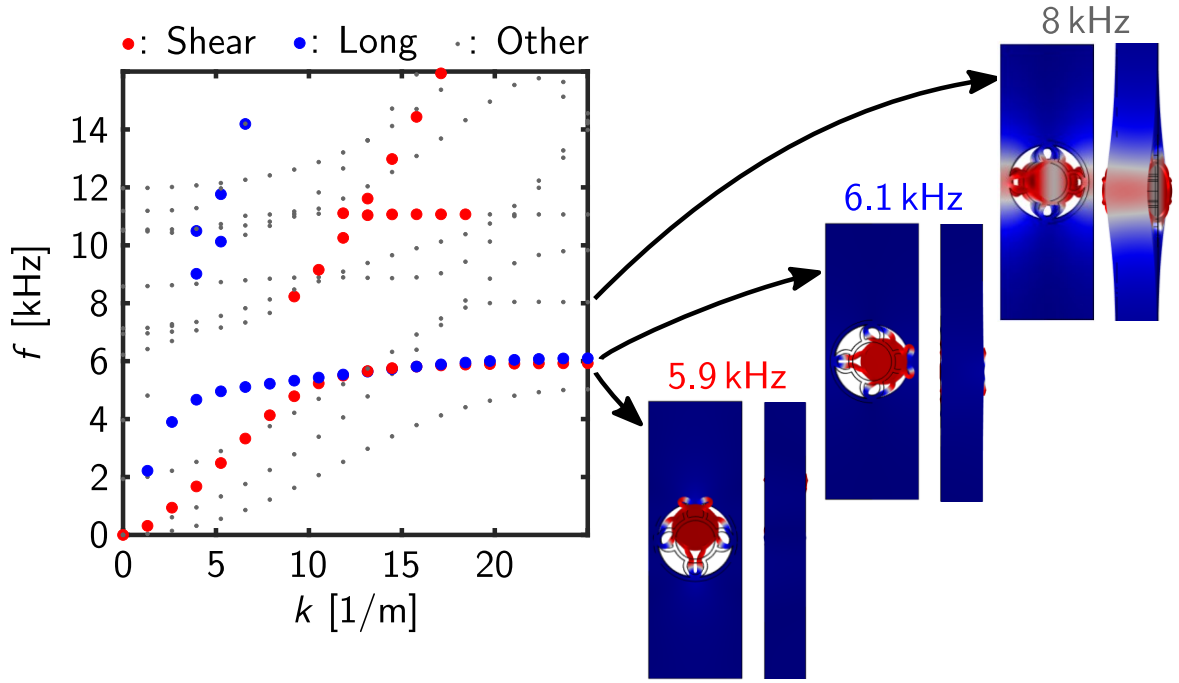

Figure 2. 12: Numerical dispersion relation of the unit cell.

As previously mentioned, the dispersion relation curves depicted in the graphic above, frequency [kHz] versus wavenumber [1/m], allow to identify specific modes of wave propagation. Additionally, each of these wave modes curve is pointed out by a series of circular markers, that are automatically color-coded depending on the characteristics of the corresponding mode shape.

The insets of the unit cell illustrate three distinct mode shapes at $k = \pi/a$: the lowest frequency, 5.9 kHz, is related to a shear mode shape, and it is characterized by clear resonant dynamics, whereby the inner 3D printed resonator moves while the acrylic substrate does not. The following mode shape, at 6.1 kHz, is instead related to a longitudinal mode shape. The inset at the highest frequency indicates an out-of-plane mode shape, featuring resonant dynamics at 8 kHz. All grey points correspond to mixed modes.

As spotlighted in the diagram, the blue markers represent a longitudinal mode of wave propagation, that features a bandgap starting at 6.1 kHz, where the mode flattens. It is important to notice that this gap is caused by resonant dynamics of the polymer-steel resonator. This is highlighted by the corresponding mode shape at the edge of the Brillouin zone, corresponding to the maximum k value.

The mode of wave propagation we are mostly interested in, is the shear mode, that is pointed out in the graphic by the red markers. Its resonant bandgap, that is the interval of frequency where no wave modes are allowed to propagate, takes place at acceptable frequencies, starting at 5.9 kHz.

2.3 Implementation of 1D finite array of resonators in COMSOL

In order to look at the transmission response, we develop a frequency domain analysis considering a 1D finite system, made by replicating the unit cell along x. In other words, the geometrical model, computed in COMSOL, is a strip composed by an array of 18 resonators. Hence, the dimensions of this strip are: 360 mm length, 60 mm height and 6.35 mm thick.

The materials assigned are the ones used for the unit cell, with the same mechanical properties, as explained in the previous section.

In the present frequency domain simulation, the frequency range we are interested in goes from 0 to 10000 Hz, setting a number of values of 100. Accuracy of the results is ensured by using convergent meshes of quadratic tetrahedral elements. Notice that our numerical simulations do not feature any damping.

To simulate the shear wave signal, a displacement of 0.1 mm is applied at the input point along y direction. Instead, if we want to send a longitudinal wave, the displacement is applied along x axis. The input point is located in the center of the first face of the strip, while the output point is centered at the opposite face, at the end of the strip, as illustrated in the following picture (Figure 2.13). Hence, this is a point evaluation analysis, that allows to derive the values of the velocity amplitude at specific points.

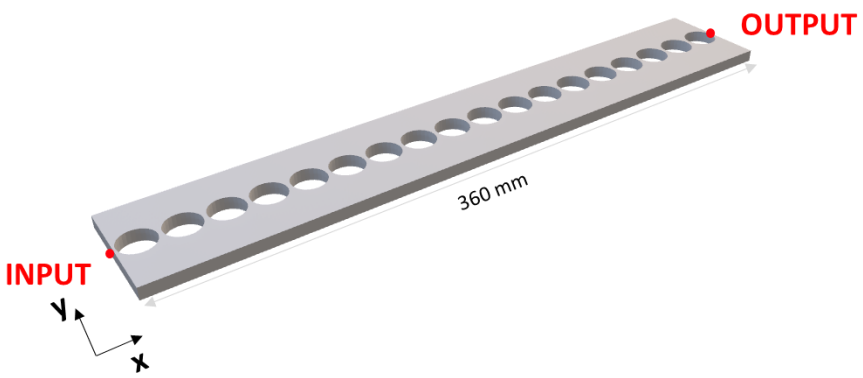

Figure 2. 13: The acrylic strip with 18 holes.

We need the response at these two target points, because we want to plot the transmissibility (TR), which is the ratio between the output velocity and the input velocity, versus frequency.

2.4 Experimental setup

The current experiments are designed to evaluate the transmission response of a seismic wave signal, at each point of an acrylic plastic strip, in which the resonators are embedded.

In this section, all the instruments used for making the measurements are described.

- Laptop
- Signal generator (Agilent 33220A)
- Piezo amplifier
- Piezoelectric actuator
- Laser Vibrometer (Polytec)
- Digital Phosphor Oscilloscope (Tektronix DPO3034)

In Figure 2.14, all these measurement tools are connected to each other with cables, powered by electricity.

The specimen is glued to a transducer, that is a piezoelectric actuator capable of generating wave signals.

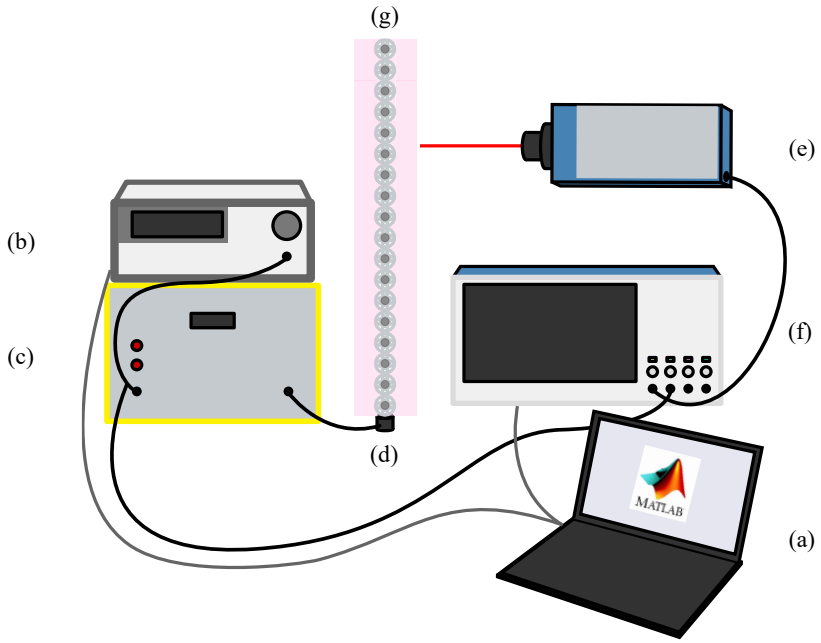

Figure 2. 14: Sketch of the experimental setup: (a) laptop with MATLAB, (b) signal generator, (c) piezo amplifier, (d) piezoelectric actuator, (e) laser vibrometer, (f) oscilloscope, (g) strip of resonators.

The signal is an arbitrary waveform, generated in a single MATLAB code as a .txt file. It is a wideband Ricker signal centered at 10 kHz, with an amplitude range between -1 and 1, while the length in time of the signal is 0.05 s (Figure 2.15).

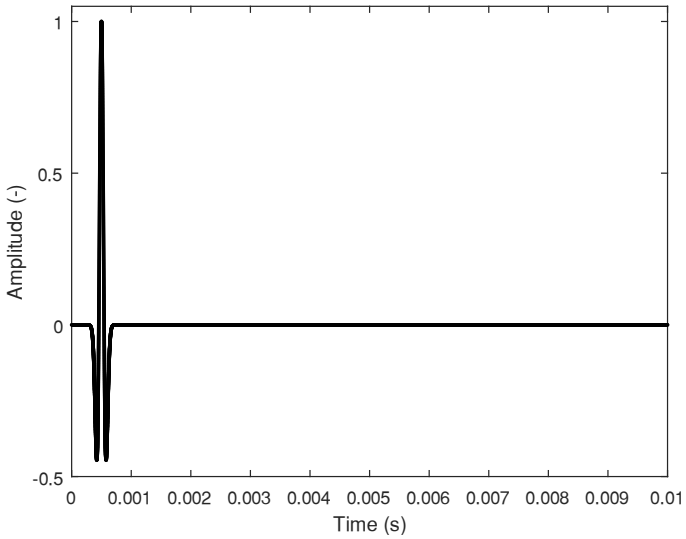

Figure 2. 15: The Ricker waveform generated with a MATLAB code.

The Ricker wavelet is theoretically a solution of the Stokes differential equation, which considers the effect of Newtonian viscosity, and is applicable to seismic waves propagating through viscoelastic homogeneous media.

In particular, Ricker wavelets are commonly used in seismology because they resemble the asymmetric frequency content of seismic waves [24].

The Ricker wavelet is defined in the time domain as:

$$r(t) = \left(1 - \frac{1}{2}\omega_P^2\tau^2\right)\exp\left(-\frac{1}{4}\omega_P^2\tau^2\right)$$

where τ is time (in seconds) and ω_p is the most energetic frequency (in radians per second). It is symmetric in the time domain and has a zero mean, as $\int_{-\infty}^{\infty} r(\tau)d\tau = 0$.

Mathematically, the Ricker wavelet is the second derivative of a Gaussian function; therefore, it is symmetric in the time domain. However, seismic signals are often not symmetric and instead are close to the first or one-and-a-half derivatives of a Gaussian function. In the frequency domain, the amplitude spectrum of the Ricker wavelet and the spectra of various derivatives of a Gaussian are asymmetric. Physically, asymmetry represents the frequency dependent attenuation behavior of seismic waves in viscoelastic media [26, 27].

As the measurement tools are concerned, the laptop is connected to the signal generator (Agilent 33220A) that receives the waveform generated with the MATLAB code, as a voltage. To

increase the power of the signal, a piezo amplifier is used. It is an electronic device that enhances the voltage of the signal generator.

The Polytec Laser Doppler Vibrometer operates on the Doppler principle, measuring back-scattered laser light from a vibrating structure, to determine its vibrational velocity and displacement. A vibrometer system is comprised of controller electronics and a non-contact standard-optic or fiber-optic sensor head. The OFV-5000 Vibrometer Controller features excellent vibration resolution and dynamic range from a choice of digital/analog decoders, remote focus and focus memory, high capacity for a wide range of modules and digital filtering. The controller provides signals and power for the sensor head and processes the vibration signals. These are electronically converted by specially developed decoders within the controller to obtain velocity and displacement information about the test structure. A system comprises an OFV-5000 controller, a choice of decoder modules and a sensor head.

The digital signal processing based adaptive filter module significantly improves the signal-to-noise ratio of the vibration signal by suppressing random and non-periodic noise for frequencies ranging from DC to 20 kHz.

A digital phosphor oscilloscope (Tektronix DPO3034) is a digital storage oscilloscope, and the same can be true in reverse. Real-time sampling simply means that the scope is able to capture signals in a single acquisition utilizing a high-sample-rate analog-to-digital converter (ADC).

2.4.1 Experimental analysis

Aiming to validate the results obtained via the numerical simulations computed in COMSOL Multiphysics, now, we proceed testing a strip with 18 3D printed resonators (Figure 2.16), where the resonating masses of steel are pressed-fit into the polyamide resonators.

Figure 2. 16: 3D printed resonators with the inner steel mass inserted.

We cut a rectangular acrylic strip, with the same dimensions of the one created in the numerical model, as described in the previous sections. As previously showed, its geometrical dimensions are 360 mm length, 60 mm height and 6.35 mm thick. Then, we drill 18 holes in the acrylic strip by using the laser cutter, that is a machine provided by our laboratory.

We are going to test the strip before without and then with the 3D printed resonators embedded and glued inside each hole. In Figure 2.17, the specimen with 18 resonators, that are pressed-fit into the acrylic strip, is illustrated.

Figure 2. 17: The strip with 18 resonators.

Hence, we are ready to test this strip by using all the instruments of the experimental setup described in the previous section.

In the following picture (Figure 2.18), all the measurement tools are assembled and connected with cables, powered by electricity. The specimen with 18 resonators is glued to a piezoelectric actuator capable of generating seismic waves.

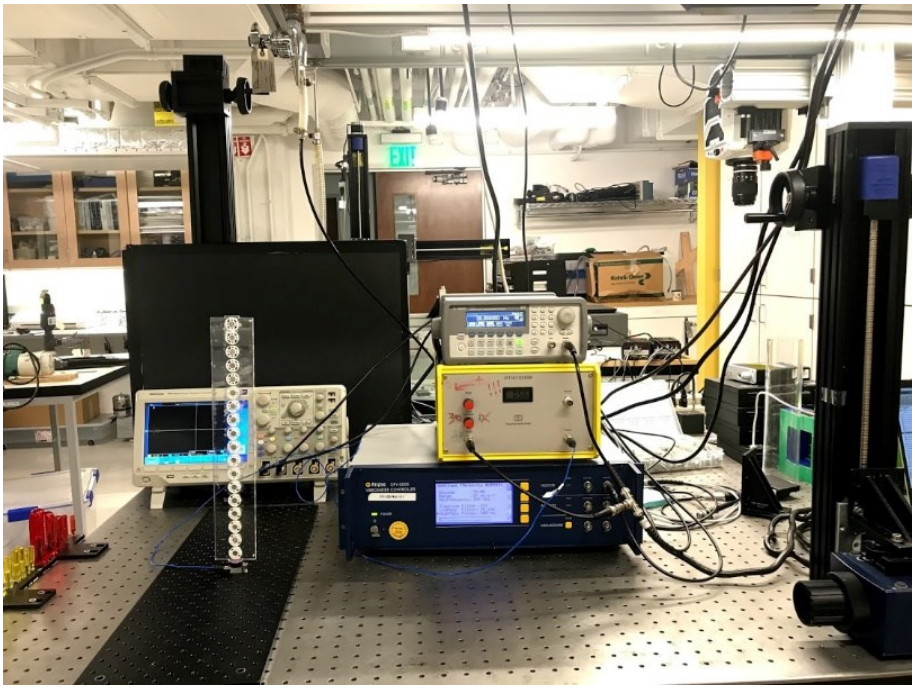

Figure 2. 18: Experimental setup during the measurements.

We investigate the propagation of seismic waves excited by a Ricker wavelet, centered at the resonant frequency of 10 kHz.

This signal, generated in a MATLAB code, is sent from the laptop to the signal generator, which is connected with a cable to the piezo amplifier, capable of enhancing the power of the signal.

To measure both the shear and the longitudinal components of traveling waves at various points of the structure, a laser vibrometer (Polytec) is used. As can be seen in the right side of the picture, the laser is fixed on a motorized linear stage, and it is possible to program the stage, in order to move it to specific locations, so the laser can acquire data at specific points.

In particular, we place a piece of retro-reflective tape in those points where we want to get the values of velocity, that is where the resonator wall is directly in contact with the acrylic material. This retro-reflective tape is used to clearly mark areas, providing a reflective light that is cast off the tape. In fact, its material is made with tens of thousands of tiny glass beads that reflect light and send a focused signal directly back to the original light source.

However, velocity signals are then recorded by an oscilloscope (Tektronix DPO3034). The data obtained from these measurements are then post-processed in MATLAB.

Since our laboratory is provided by different types of piezoelectric actuators, consequently we have the possibility to test the specimen both sending longitudinal and shear wave signals.

Indeed, if we want to look what happens when a shear wave is sent from the bottom, we need to glue the specimen to the piezoelectric actuator for shear signals. The laser is located horizontally sideways, as in Figure 2.18, measuring from the side at different locations of the array of resonators in a way that is orthogonal to the direction of wave propagation.

Contrarily, if we want to send a longitudinal wave from the bottom of the strip, we need to glue it to the piezoelectric actuator for longitudinal signals. In this case, the laser is located above and rotated vertically, making the measurements longitudinally to the direction of wave propagation.

To sum up, in both cases, by measuring at each point of this array of resonators it is possible to reconstruct the experimental dispersion relation curve and make a comparison with the numerical one obtained from the eigenfrequency analysis of the unit cell.

Acquiring data at the top (output point) and at the bottom (input point) of the array, we plot the transfer function versus frequency, in order to get the transmission response.

2.5 Numerical and experimental results

We are interested in reconstructing the experimental dispersion relation curve by recording the values of velocity measured at each single resonator of the strip. The reconstructed dispersion relation dotted curve allows to detect the width of the bandgap in the frequency versus wavenumber diagram, and to identify the frequency of resonance of the system.

In this section, a comparison between the results obtained from numerical simulations computed in COMSOL Multiphysics and the measurements made with the tabletop experimentation are illustrated.

2.5.1 Shear wave experiment

As for the shear wave experiment is concerned, the numerical dispersion relation curve, obtained in COMSOL by analyzing the unit cell with Bloch-Floquet boundary condition, is illustrated in Figure 2.19. The red markers show the shear mode of wave propagation, highlighted by using an index in a MATLAB code. In the background of this graph is possible to observe the reconstructed dispersion relation for the medium via a 2D-Discrete Fourier Transform of the space-time data we obtain. Hence, it is a colormap where the darker regions match well with the markers corresponding to the numerical dispersion relation especially around the point where the lower shear branch flattens, that is near resonance.

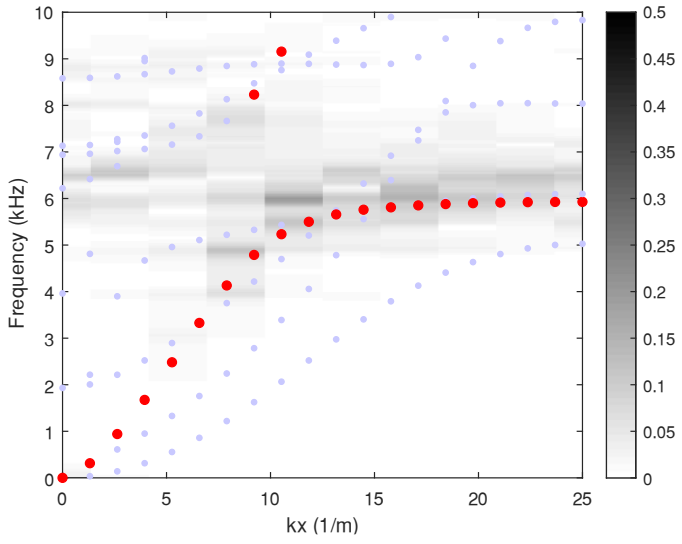

Figure 2. 19: The dotted curve is the numerical dispersion relation for the shear wave propagation, while the colormap in the background is the experimental dispersion relation.

Predicting the full width of the bandgap from this plot is very difficult. For this reason, to better extract this information, we plot the transmissibility. As previously explained, we consider only the measured data at the input, near the transducer, and at the output, that is the point of the specimen that is further away from the actuator.

The transmissibility diagram, shown in Figure 2.20, is frequency [kHz] versus the transfer function, that is nondimensional, which is the ratio between the values of velocity at the output point over the ones at the input point. Moreover, the black curve is the numerical transmissibility, while the red one is the experimental transmissibility.

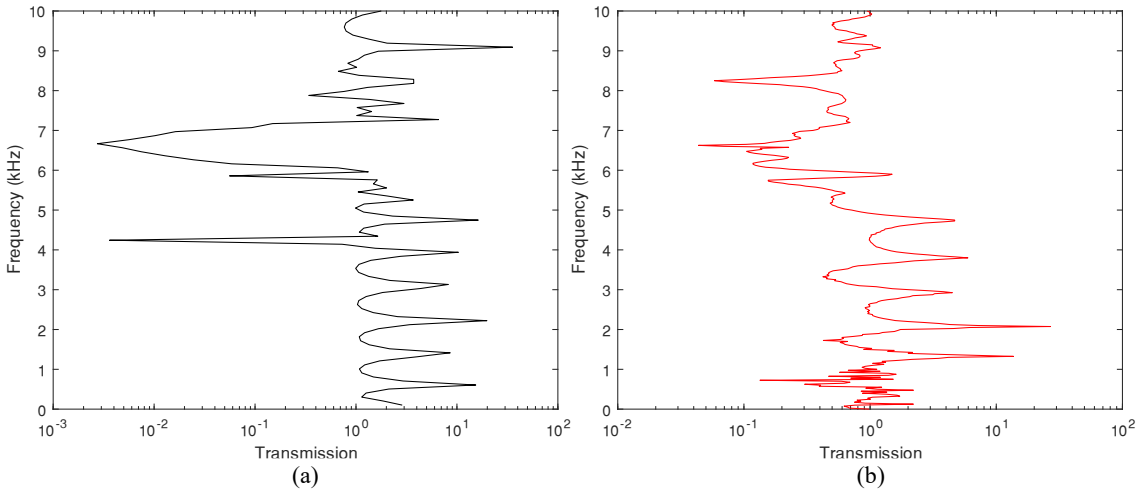

Figure 2. 20: (a) The numerical transmissibility. (b) The experimental transmissibility.

From these two diagrams, it is possible to observe that the numerical model captures the experimental response for a wide range of frequencies. In fact, this is highlighted by the proximity of peaks in the two sets of results. Additionally, both numerical and experimental results show a dip in the transmissibility between 6 and 7.3 kHz, which can be ascribed to the bandgap.

2.5.2 Longitudinal wave experiment

In this section, the diagrams related to the longitudinal wave experiment are reported.

Both the numerical and experimental dispersion relation curves are illustrated in the following diagram (Figure 2.21). Also in this case, the colormap in the background shows that there is a

match between the two trends. In fact, the darker regions follow exactly the path of the red dotted branch, pointing out the bandgap, that starts at 6.1 kHz.

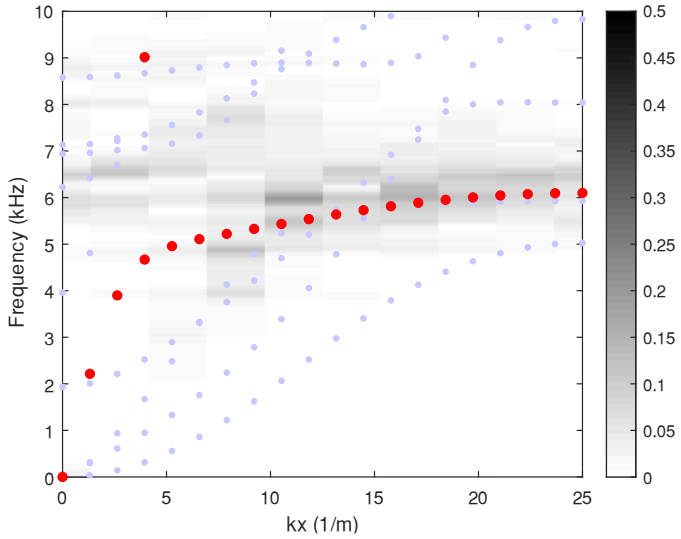

Figure 2. 21: The dotted curve is the numerical dispersion relation for the longitudinal wave propagation, while the colormap in the background is the experimental dispersion relation.

The extent of the bandgap can be better highlighted if we look at the transmission response of the longitudinal wave experiment.

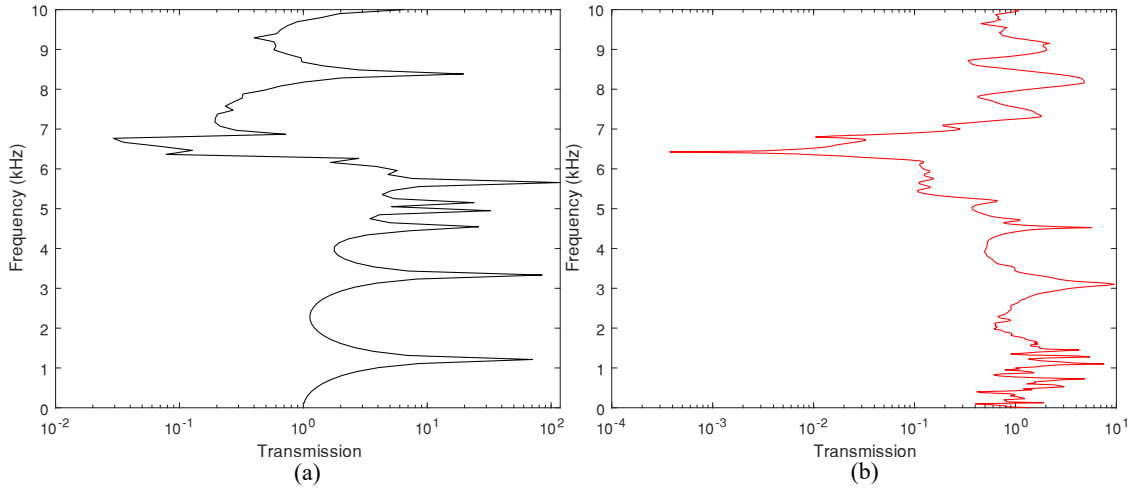

Figure 2. 22: (a) The numerical transmissibility. (b) The experimental transmissibility.

While in the numerical transmissibility, the bandgap starts from the peak at 5.6 kHz to the one at 8.3 kHz, in the experimental diagram, the dip goes from 4.5 kHz to 7.3 kHz, as shown in Figure 2.22.

So, there is a match between the two frequency ranges where no wave modes are allowed to propagate.

While these longitudinal results are not strictly of interest for the present work, they further highlight the fact that the behavior of these 3D printed resonators is accurately characterized by our numerical models.

Chapter 3
Experiments on shear wave attenuation via metapiles

3.1 Introduction

The purpose of this master thesis is to provide an experimental proof-of-concept of seismic wave attenuation through metapiles. Metapiles can be considered as one-dimensional arrays of resonators located beneath the surface of a half-space.

The resonators are placed below the surface of the half-space and around the target location, where is supposed to be the critical building or the area that needs to be protected from earthquakes.

After testing the behavior of our 3D printed resonators via eigenfrequencies and transmission analyses in COMSOL Multiphysics and validating the results by tabletop experimental simulations considering the strip of one-dimensional array of resonating units, we now want to test the idea of wave attenuation via metapiles.

In this chapter, we provide an experimental demonstration of the attenuation behavior of arrays of our composite resonators embedded in a larger acrylic domain. While this idea could be applied to 3D domains, we choose to validate it for a 2D medium for simplicity.

We are particularly interested in the physical demonstration of a minimalistic case, in the sense that we try to minimize the number of resonators employed in each metapile.

We prove that sparse arrangements of engineered vertical pillars of resonating metamaterials allow to significantly attenuate seismic waves that travel from the depth direction, that is the source of the signal, to the target location of a reference point.

3.2 Experimental setup featuring the larger acrylic domain

To simulate the scenario where arrays of resonators are embedded in a wider domain and are located around a target point on the surface of the medium, we consider a big acrylic plate, as shown in the sketch in Figure 3.1. In this configuration, the behavior of the resonators is not significantly affected by the presence of the lateral boundaries, since these are relatively far from the resonators.

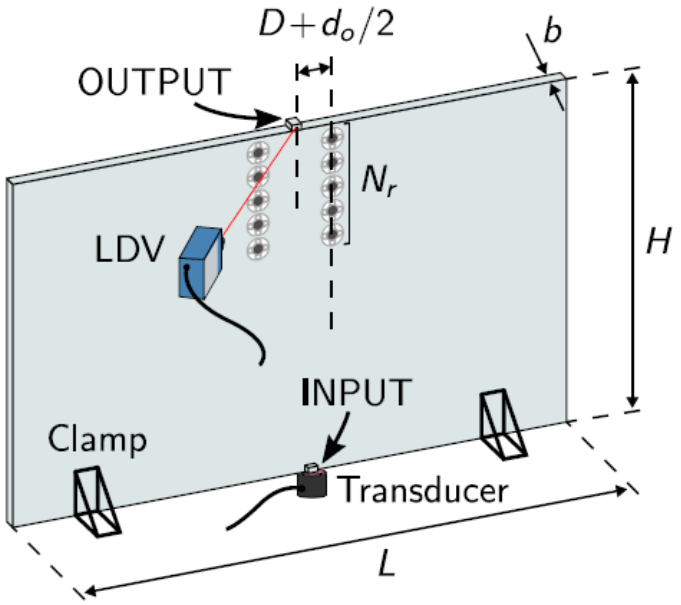

Figure 3. 1: Sketch of the experimental setup, featuring a large acrylic plate with two metapiles.

In this picture the experimental tabletop setup for our experiment is clearly illustrated. Notice that the same measurement tools used to test the 1D array of resonators are used in this experiment as well. In fact, also in this case, we need the laptop with the MATLAB code to send the Ricker signal, the signal generator (Agilent 33220A), the piezo amplifier, the piezoelectric actuator, the laser vibrometer (Polytec) and the oscilloscope (Tektronix DPO3034).

Our specimen features two piles in which five resonators are vertically aligned, that are embedded in the acrylic plastic (PMMA) plate, whose mechanical properties are: Young's Modulus E = 5.5 GPa, Poisson's ratio $\nu = 0.35$ and density $\rho = 1190$ kg/m^3.

Additionally, the geometrical dimensions of the acrylic domain are width L = 1219 mm, height H = 610 mm and thickness b = 6.35 mm.

Since the acrylic plate is bigger than the strips cut by means of the laser cutter for the 1D experiment, now we need another machine to drill holes in it: the CNC router, that is a computer-controlled cutting machine. It typically mounts a hand-held router as a spindle which is used for cutting various materials, such as wood, composites, aluminum, steel, plastics, glass, and foams.

By using a CNC router, we carve ten holes in the acrylic plate, and then we press-fit the composite 3D printed resonators inside them. The resonators design is the one described in section 2.2.5.

Hence, the two metapiles of five resonators each are placed right below the top edge of the acrylic domain. In particular, the center of the first resonator is located at $a/2$ from the top edge. Moreover, the edge of the resonator of each pile is located at a distance D from the vertical mid-line of the acrylic plate, while the distance between the center of the resonator and that mid-line is $D + d_0/2$.

Since we know that the diameter of each resonator d_0 is 18 mm, for this tabletop experiment, we choose D = 21 mm. The value of D is chosen so that the distance between the two piles 2D= 42 mm is much smaller than the wavelength we expect at the resonant frequency of the resonators, 223 mm.

Therefore, all the system is fixed to an optical table by means of two clamps, that are located at 30 cm from both lateral sides of the plate at the bottom edge.

Since we perform a transmission experiment, we need to record the response values at the output and at the input points, in order to obtain the transfer function that is the ratio between them. These points are located along the vertical midline of the plate.

In particular, the input point is located in the center of the bottom edge of the plate, exactly where the input signal is recorded. As previously explained, since we want to simulate a source for seismic waves, we glue the transducer at the input point. We use the same transducer of the 1D array of resonators experiments. Moreover, we need to provide a measurement point for in-plane shear waves that is accessible to the laser vibrometer. For this reason, we also attach a small acrylic block onto the plate near the transducer. This measurement point is used to record the input signal.

In fact, the laser vibrometer needs to be parallel to the direction of wave propagation one intends to measure.

Instead, at the top edge of the plate, that represents the free surface of our domain, we also glue an acrylic block, that is needed to record the output shear response.

To properly record in-plane shear waves, the laser should be parallel to the plate itself. However, this is not possible due to space limitations in our tabletop laboratory setup. As a consequence, the laser is oriented at $\propto \approx 30°$ angle with respect to the plate and is therefore bound to record some out-of-plane dynamics together with the desired in-plane vibration.

Particularly, the following picture shows the experimental setup for the shear wave tabletop experiment in our laboratory. As shown in Figure 3.2, the acrylic plate is fixed by means of two clamps to the optical table of our laboratory. From the insets, it is shown that ten 3D printed resonators are pressed-fit inside the holes. The two metapiles are located at a distance of 21 mm from the target point, that is the output point. While the transducer for shear wave signals is glued at the input point.

The laser is fixed on a motorized linear stage that is computer-controlled and oriented towards the points of interest, highlighted by the red circles, where the two acrylic plastic blocks are glued in order to facilitate the measurements.

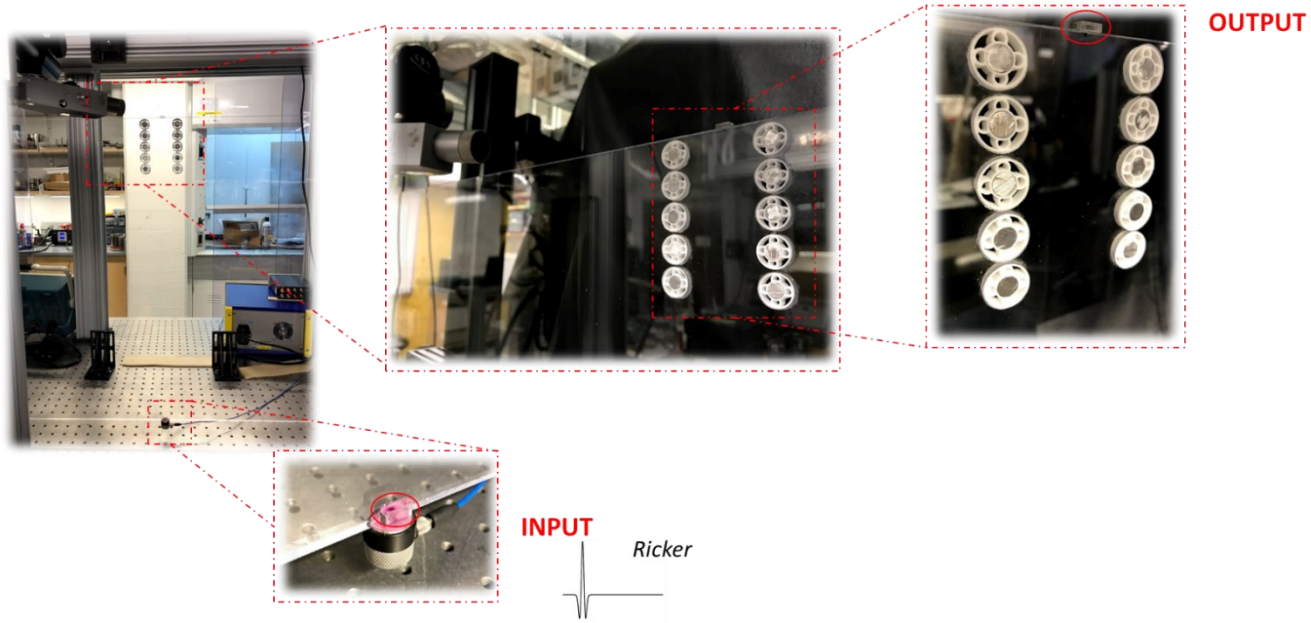

Figure 3. 2: Experimental setup for shear wave experiment on the acrylic plate with two piles of resonators.

3.3 Implementation in COMSOL

To provide a complete characterization of the measured data, we implement the system in COMSOL Multiphysics. Hence, the geometry of the system is replicated in the numerical model, where the acrylic plate is reproduced as a big block with the same dimensions of the real one: width L = 1219 mm, height H = 610 mm and thickness b = 6.35 mm. At 300 mm from both lateral sides of the plate, there are two joints, that fix the system.

The distance between the two vertical metapiles with five resonators each is 42 mm as well. The resonators diameter is 18 mm, and they are modeled as previously described.

We perform a harmonic analysis to also determine the transmissibility of this medium to in-plane shear waves.

3.4 Numerical and experimental results

In this section, numerical and experimental results of the transmission analysis of the acrylic plate with two columns of resonators are compared. Hence, the transmissibility curves are reported in Figure 3.3.

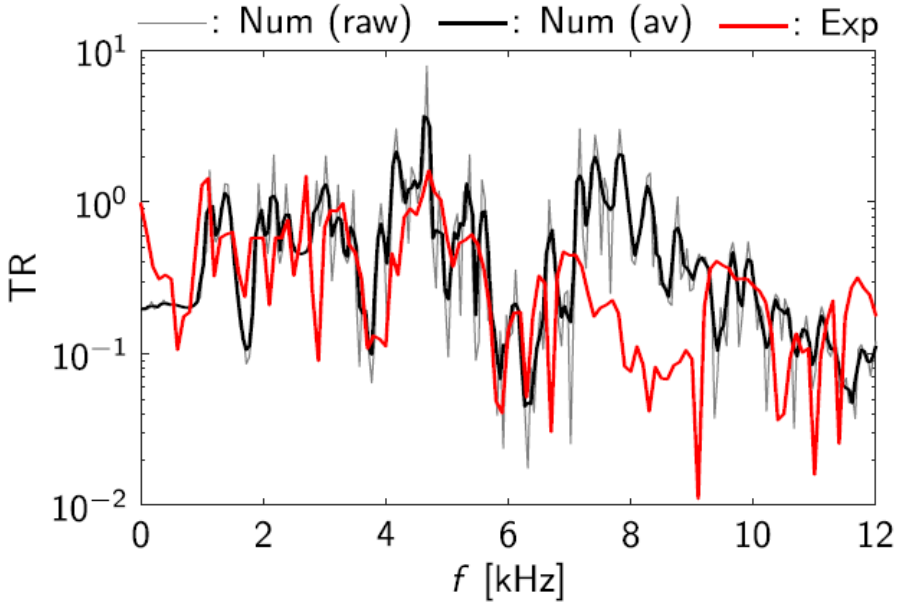

Figure 3. 3: Numerical and experimental transmission curves.

In the numerical simulation we do not consider any damping. Moreover, to smoothen-out the numerical frequency response and to make it resemble the response one would obtain with moderate values of damping, we apply a moving average filtering procedure. A moving average is a technique to get an overall idea of the trends in a data set; it is an average of any subset of numbers.

The graphic of Figure 3.3, where there are three different colored curves, shows a comparison between the experimental and the numerical transmissibility of this medium.

In particular, the responses before and after the application of the moving averages are shown respectively as black and grey curves, while the red curve refers to the experimental transmission curve. Thus, the averaged numerical curve is obtained from a moving average of the raw data.

The experimental result, due to the limitation of our setup, account for both-in-plane and out-of-plane motion.

It is possible to notice that the numerical and experimental curves match nicely up until 7 kHz. Both sets of data capture the small dip around 4 kHz. Moreover, the amplitude increases around 5 kHz, and the large dip starts right below 6 kHz, that is ascribed to the bandgap.

Based on our knowledge on the dynamics of these resonators, we understand that this large dip is the onset of the bandgap induced by the shear resonance within the resonators of the metapiles. After a frequency of 7 kHz, we can see that the numerical response increases again, while the experimental one experiences a second large dip. We claim that this second dip is due to undesired out-of-plane dynamics of the plate that are picked up due to the fact that the laser is oriented at a 30° angle.

This conjecture is corroborated by the fact that the band diagram that represents the dispersion relation of the unit cell, reported in Figure 2.12 in section 2.2.6, shows that our resonators present an out-of-plane resonance in the neighborhood of 8 kHz, the frequency at which we see a second dip in Figure 3.4.

In conclusion, this preliminary experiment demonstrates that a good attenuation will take place in the frequency range of interest, between 6-7 kHz, even if we use spaced-out arrays of resonators.

In the following sections, we will use numerical simulations to better understand this attenuation phenomenon.

3.5 Numerical generalization and parametric study

For a deeper understanding of the effects of various metapile parameters into the attenuation performance, we need to study and test many different arrangements of resonators.

Since this is not very easy to do experimentally, since each tested configuration would require a separate specimen, we implement the model in COMSOL Multiphysics.

In previous section we have validated the numerical simulations by means of experimental results for a specific choice of resonator parameters, now we want to extend the numerical study by testing different resonators configurations.

We keep the same identical resonator design described in section 2.2.5 and we compute different models varying D, the distance between the inner edge of a metapile and the target location to be isolated, and the N_R, the number of resonators in each metapile.

Instead of applying a point source as in the previous numerical simulations, here we apply a line load to simulate a shear force at the input point. The line load is applied along a line that is perpendicular to x axis, through the thickness of the plate. Additionally, we apply fixed edge boundary constraints at 300 mm from both lateral bottom edges of the plate.

To compare the performance of various configurations, we define a metric of wave attenuation performance as shown in Figure 3.4 (a, b).

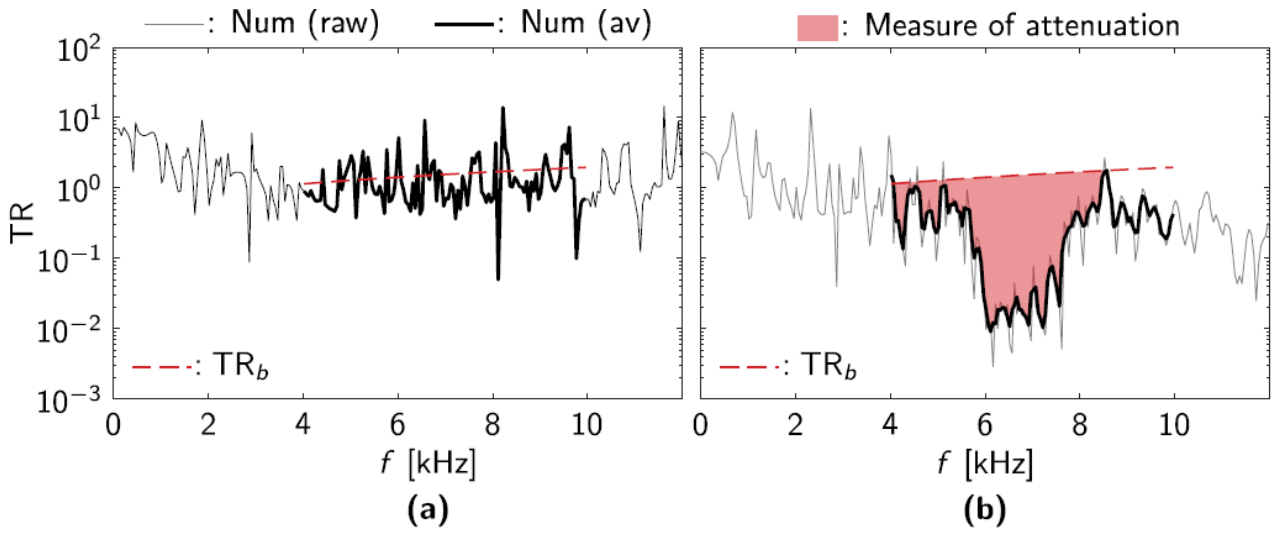

Figure 3. 4: (a) Transmission curve of the bare plate, without resonators. (b) Extraction of the attenuation measure from the transmission of a configuration with resonators.

Note that identifying the extent and magnitude of bandgaps from the response of a finite structure is typically challenging.

TR_b is the baseline transmission in the 4-8 kHz range of interest, obtained by fitting the transmission with a first order polynomial. The configuration related to the diagram in Figure 3.4 (b), featuring 20 adjacent piles with five resonators per pile, is used as reference to benchmark attenuation performance. The shaded area is obtained by intersecting the transmission with the TR_b line.

First, we consider the frequency range where there is supposed to be the bandgap, that goes from 4 kHz to 10 kHz. We compute the transmission analysis of a bare acrylic plate without resonators, from which we extract a baseline curve, that is a linear fit of the response in the desired frequency range. In this way we take into account the slope of the response curve in the range of interest.

In other words, when we study a system without resonators, we first smoothen out the numerical transmissibility with a moving average filter and then, we consider as bandgap the region that includes the expected resonance of 6 kHz and that remains below the baseline. The area of that region is our measure of attenuation.

The attenuation area obtained for each metapile configuration of interest is normalized by the area obtained for a compact array of $20\ x\ 5$ resonators located right below the target location to be isolated.

Figure 3.4 (b) shows the transmissibility and the attenuation area for this reference configuration, that is akin to a metafoundation.

The combinations of parameters of interest for this study are: $D\ (cm) = 0.25, 1, 2, 3, 4$ and $N_R = 1, 3, 5, 7, 9$. By considering the normalized areas for each of them, we can extract information to compute the design map shown in Figure 3.5.

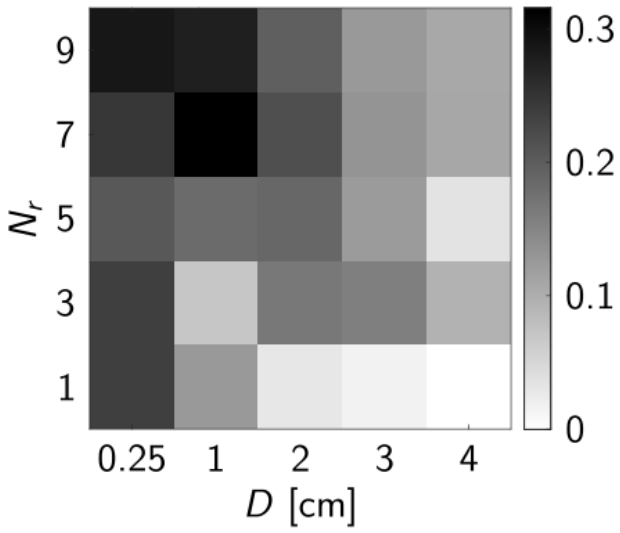

Figure 3. 5: Evolution of the attenuation performance with N_R, the number of resonators in a metapile, and D, the distance between the edge of one metapile and the output measurement point. The attenuation measure for each case is normalized by the area of the benchmark in Figure 3.4 (b).

To better appreciate the extent of the attenuation area for each metapile configuration, we can study the transmission plots illustrated in Figure 3.6. In particular, we notice that configurations with more resonators in the metapile and with less distance between piles perform better in terms of wave attenuation. Furthermore, their performance is approximately 30% of the performance of a metafoundation featuring a number of resonators an order of magnitude larger than any metapile configuration.

From these plots, it is clear that D has much larger effects than N_R. In fact, configurations with metapiles close to each other but featuring few resonators perform better than configurations with many resonators per pile but with far-away piles.

This is not surprising since, for D = 4 cm, the distance between piles of 2D is now on the same order of magnitude as the wavelength for shear waves inside the acrylic plate, and waves are bound to sneak in between the metapiles.

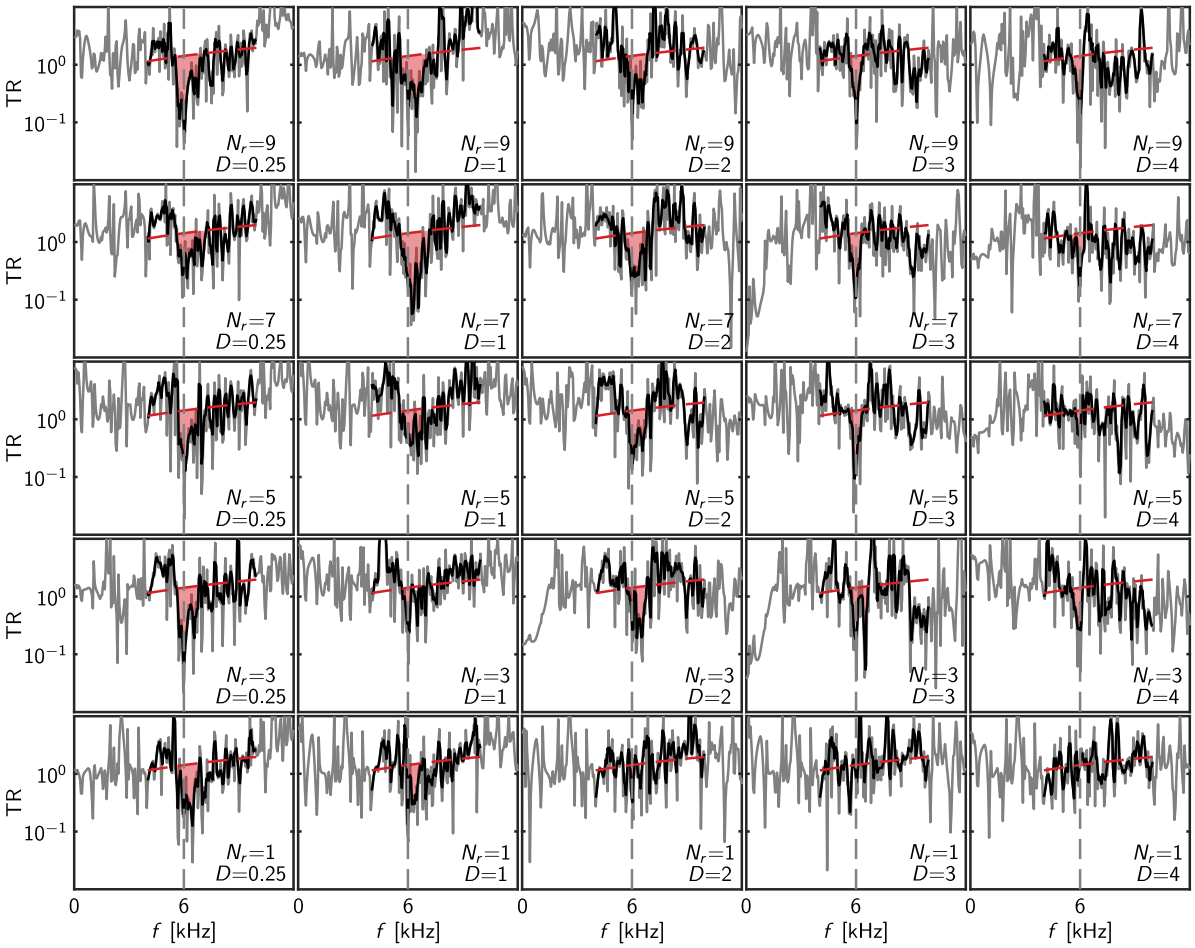

Figure 3. 6: Complete map of the transmission results that yield the parametric colormap in Figure 3.5. All simulations feature a line wave source.

Chapter 4
Numerical simulations in a soil-like medium

4.1 Problem statement

After explaining the fundamental idea behind the concept of metapiles, we now apply this knowledge to a case study that can represent a potential application of this idea.

We consider a portion of the surface of the Earth, where there is supposed to be a structure that we want to isolate from seismic waves. A key issue of this problem is that we want to shield the building from bulk shear waves that travel from the depth direction towards the surface.

In order to gain a good attenuation of shear waves and to protect the structure from surrounding vibrations, researchers have thought about using seismic resonant metamaterials.

The schematic depicted in Figure 4.1 summarizes the problem we are interested in. Moreover, the inset serves as a reminder that the resonator can be schematized as a mass-spring-dashpot system.

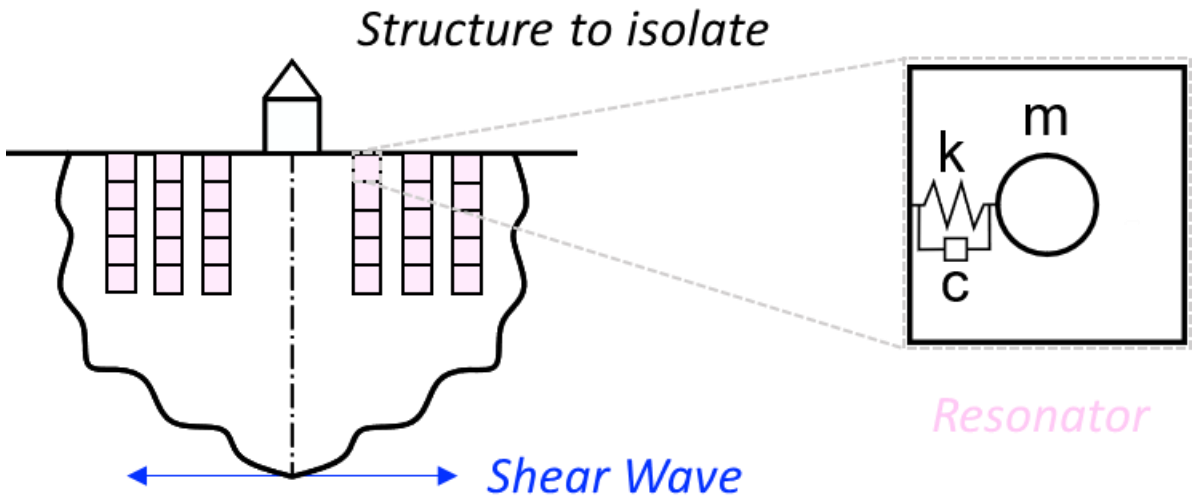

Figure 4. 1: Sketch of the problem statement.

Besides identifying the best resonator design and parameters, we want to answer the following question: “What is the minimum number of resonators to obtain a good attenuation?”.

As engineers, we are deeply interested in the feasibility of this novel seismic isolation system based on metamaterial concepts for the reduction of ground motion and vibrations when an earthquake occurs. Additionally, looking for the most minimalistic configuration of metapiles is extremely appealing to us for the realization of cost-effective metamaterial-based devices.

In this section, we want to introduce the reader to another greater outlook of the potential application of metapiles, as shield for critical infrastructures. In other words, instead of performing the parametric studies illustrated in previous sections, here we concentrate on a case study that is closer to the possible installation in the ground.

If up until now we have considered the acrylic domain with the 3D printed resonators embedded, now we extend our study to a wider half-space domain that can be seen as a half-space whose mechanical properties are the typical of a soil, where the metapiles would be buried.

Hence, we scale up our system as if we consider a portion of the surface of the Earth, that we want to isolate from earthquakes.

At this scale, the 3D printed resonator behavior is similar to a tuned mass damper, that has been used for engineering applications for a long time, for instance one of the most famous is the one inside the building Tapei 101 (Figure 4.2).

(a) (b)

Figure 4. 2: (a) The building Tapei 101 (Taiwan). (b) The tuned mass damper inside the building Tapei 101.

A tuned mass damper, also known as a pendulum damper, is a pendulum or gravity-based oscillator which is attached to the structure and it counteracts the vibration of one or more fundamental modes, reducing the seismic response.

Hence, we have thought about a potential configuration of a feasible resonator that could be vertically installed underneath the surface of the Earth as to create metapiles. As we know, the fundamental components of a tuned mass damper are mass, spring and damper. Since its behavior is similar, we can call the resonator, tuned mass damper, because it is a system designed to remove some vibrations from the surroundings at a certain frequency.

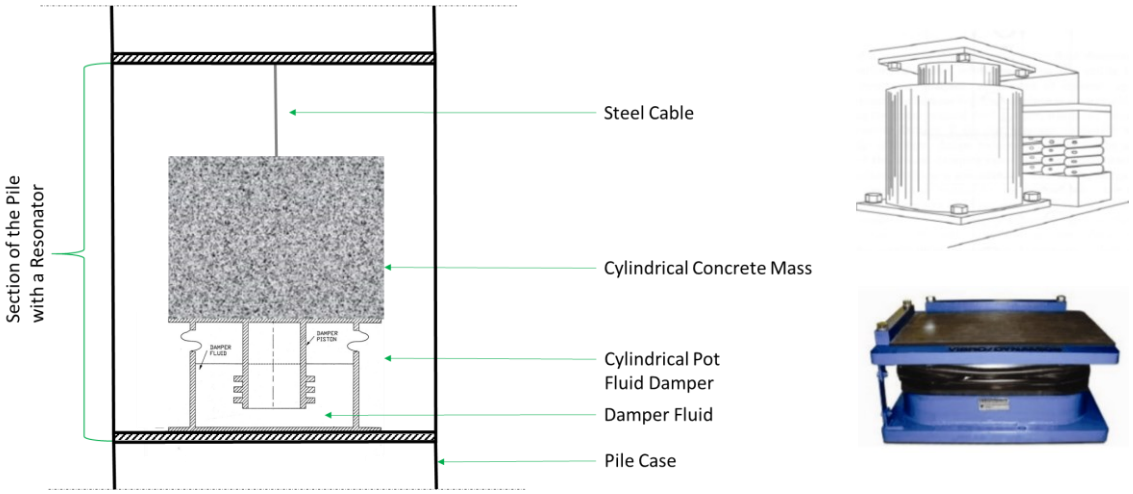

Figure 4. 3: Potential design of our tuned mass damper. Sketch by *Andrea Calabrese* at Cal State Long Beach.

Figure 4.3 shows a section of the metapile with a sketch of the proposed resonator design. Hence, a cylindrical mass of concrete is hung by a steel cable that acts like a horizontal spring, as a pendulum. The mass is supported by a damper piston inside a cylindrical pot, filled by a damper fluid.

In light of these considerations, we want to study the effects of seismic wave attenuation by considering different arrangements of metapiles.

In the following sections, we model the soil and the resonators in SAP2000, then we perform a steady state analysis to get the transmission response.

4.2 The model of a soil-like properties medium in SAP2000

The numerical platform that allows us to implement the system is SAP2000, that has many different features for structural dynamics analysis and design.

SAP2000 is a Finite Element general-purpose civil engineering software ideal for the analysis and design of any type of structural system. Basic and advanced systems, ranging from 2D to 3D, of simple geometry to complex, may be modeled, analyzed, designed, and optimized using a practical and intuitive object-based modeling environment that simplifies and streamlines the engineering process [46].

However, we implement the model of the soil by means of the software SAP2000, considering a 2D version of a 3D problem. Basically, we want to simulate an elastic half-space characterized by soil-like properties. We focus on a slice of the soil, without considering any infinite domain.

In particular, a 2D finite domain model of the half-space is implemented, and the damping boundary conditions applied to its edges simulate the presence of an infinite domain.

In order to do this, we need to create a 2D mesh of four-nodes elements of size 1 m by 1 m. In this first step, we model the soil without any resonators, while in the following step we are going to introduce the tuned mass dampers arranged according to metapiles in the soil domain.

First of all, we consider a portion of the half-space, modeled as a rectangular whose geometrical dimensions are 400 m by 20 m. This choice comes from the literature, from which we know that since we want to reduce wave reflections at the lateral boundaries of the domain, the lateral extension of the rectangular domain should be more than eight times its height [28].

In Figure 4.4, the schematic of the model of the soil without resonators is reported. Moreover, we assume plane strain conditions and a damping ratio of 5 %.

The half-space is considered linear elastic, isotropic and homogeneous. These are all strong assumptions for a soil, but they let us concentrate on the behavior of the metapiles; of course, future studies could affect these shortcomings.

The soil is modeled by shell elements with dimension 1 m by 1 m, to which we assign the mechanical properties typical of a Category B soil: Young's Modulus E = 7.072 GPa, Poisson's

ratio ν = 0.3 and density ρ = 1700.6 kg/m^3. From literature, we know that a Category B soil is a benchmark that is used for all seismic characterizations.

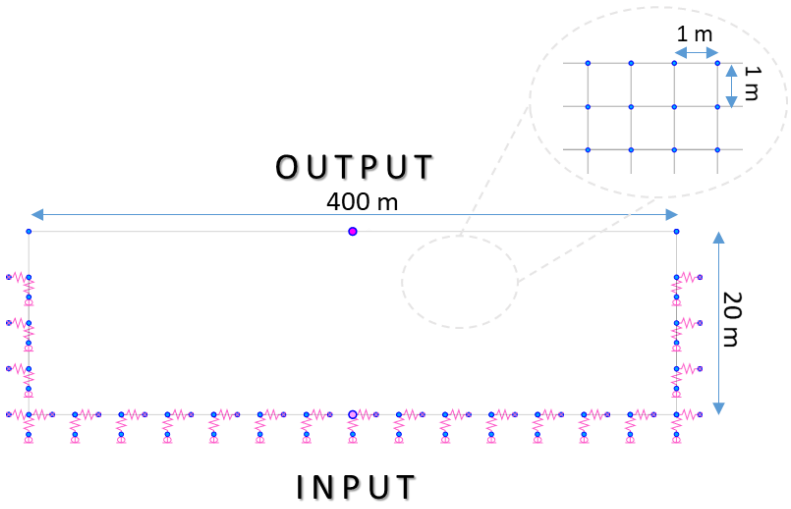

Figure 4. 4: Sketch of the model of the soil without resonators in SAP2000.

Frequency domain analyses are performed allowing us to study the harmonic response of the system. We apply a horizontal harmonic base displacement of 0.05 m along the x direction at the input point, that simulates the signal as a shear wave traveling from the depth direction.

We select the frequencies of excitations in a range from 0 to 25 Hz. We place dashpots both along the horizontal and vertical directions of the boundary domain. These have damping constants of values $c_1 = 1\,Nsm^{-1}$ and $c_2 = 0.25\,Nsm^{-1}$. Additionally, these boundary conditions assure a reasonable wave absorption and allow to reduce the reflections of waves and surrounding vibrations [29, 30].

The size of the mesh is selected to meet requirements by *Lysmer* and *Kuhlemeyer* [31] as each element has dimensions much smaller than $\lambda/8$, where λ is the wavelength corresponding to the maximum frequency of interest f.

For the analyses discussed in this work:

$$\frac{\lambda}{8} = \frac{v_s}{8f} = 16\,m$$

being $v_s = 396\,ms^{-1}$ and $f = 3.1\,Hz$.

We are interested in studying the transmissibility diagram, which is the transfer function versus frequency. To determine the transfer function, we need to compute the ratio between the value of the lateral displacement recorded at the output point, also known as the control node, that is the location to be isolated, divided by the displacement at the input point.

As for the study of the half-space without resonators is concerned, a comparison between the peaks of the numerical transmission and the theoretical solution available in the literature [32] is shown in Figure 4.5. Notice that these two curves match perfectly.

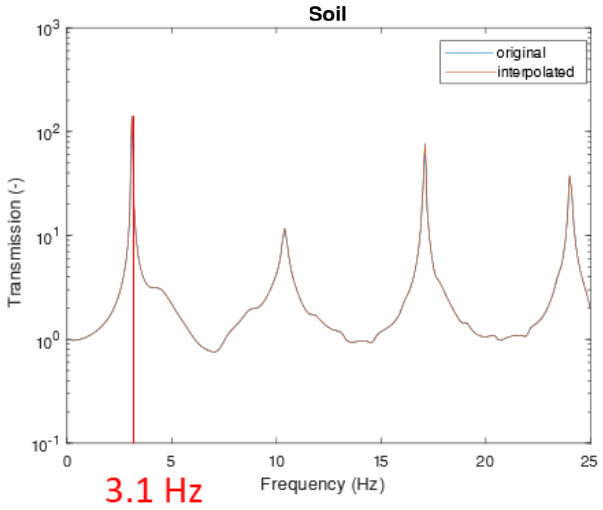

Figure 4. 5: Transmissibility diagram of the model of the soil without resonators.

The transmissibility diagram shows that the frequency of resonance of the half-space corresponds to the first peak of the curve, that is 3.1 Hz. This represents the first shear resonant frequency of the half-space, and it is the frequency of interest.

Furthermore, the resonant frequency of 3.1 Hz corresponds to a period of 0.32 s, that is in the range of typical masonry or ordinary reinforced concrete buildings.

Our purpose is to design resonators capable of attenuating waves and vibrations at 3.1 Hz, that is the frequency at which the tuned mass dampers are tuned to resonate.

In order to attenuate the 3.1 Hz peak, we introduce metapiles in the model, as arrays of resonators located at prescribed nodes of the mesh. In particular, each resonator occupies an area of 1 m by 1 m. Additionally, since a resonator can be defined as a mass-spring-dashpot

system, it is modeled as a mass and a horizontal spring, to which we assign specific mechanical characteristics, depending on the frequency and the damping.

If we put tuned mass dampers that resonate at 3.1 Hz everywhere in the half-space, we obtain the maximum attenuation of the shear wave signal that travel from the input point to the output point. In this second step, a horizontal displacement of 0.05 m is applied at the input point, as well. Figure 4.6 shows a schematic that represents the model of the soil with resonators inserted all over the half-space.

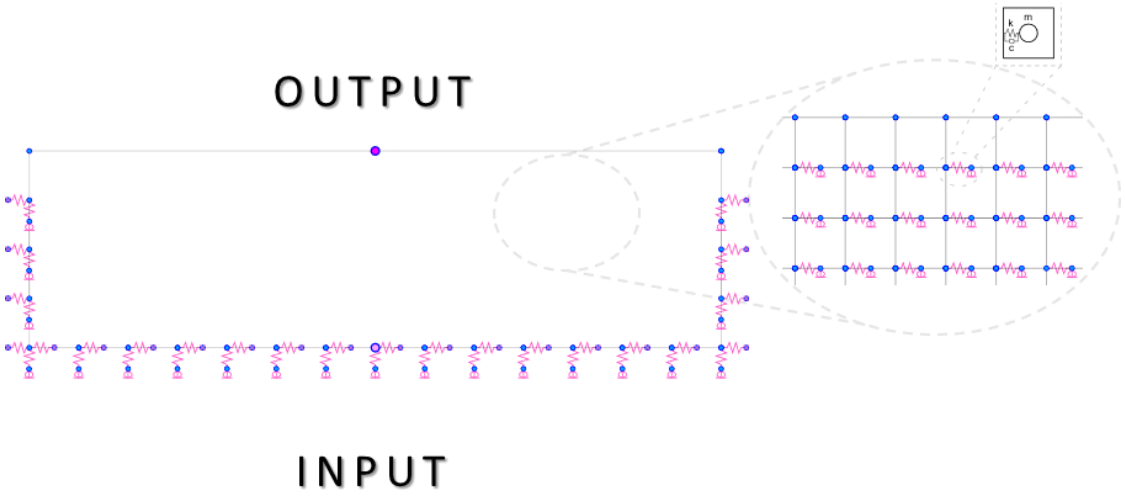

Figure 4. 6: Sketch of the model of the soil with resonators in SAP2000.

However, the harmonic analysis is computed, and the diagram obtained is shown in Figure 4.7, where the orange curve refers to a configuration featuring five rows of resonators located below the whole upper boundary of the domain, while the blue one relates to the transmission response of the soil without resonators. Notice that the resonators located everywhere in the half-space act like a single tuned mass damper; in fact, the original peak of the half-space is replaced by an anti-resonance, as a result the attenuation of the first peak produces two adjacent and distinct peaks.

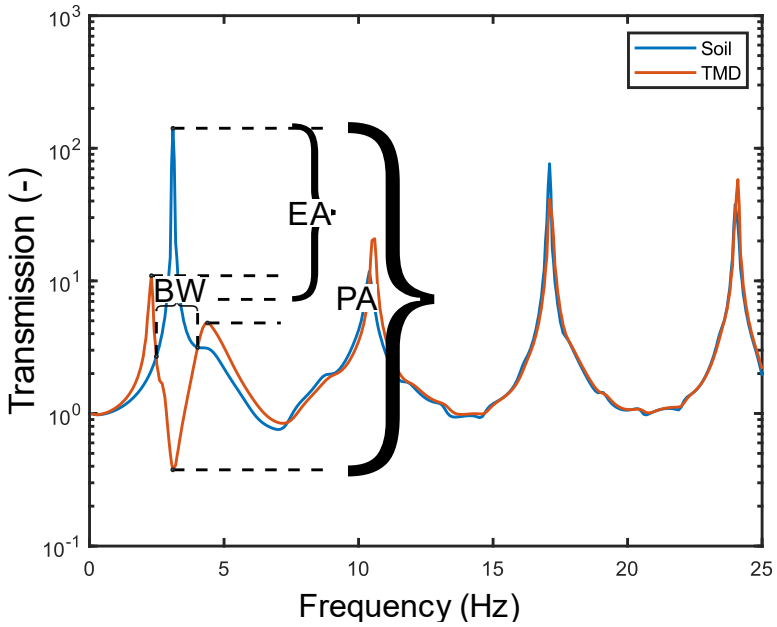

Figure 4. 7: Transmission response of the model of the soil without resonators (blue curve) and transmission response obtained from the model of the soil with resonators everywhere (orange curve).

In order to quantify the effects produced by the resonators on the response of the model, we analyze the following metrics: the peak attenuation (PA), the effective attenuation (EA) and the bandwidth (BW).

The peak attenuation (PA) is the difference between the height of the first peak of the model without resonators and the height of the peak attenuated by the resonators at the same frequency of 3.1 Hz. Moreover, the peak attenuation is important because it tells us at which peak there is the maximum attenuation, but it does not account for the fact that reducing the amplitude of the peak at 3.1 Hz increases the amplitude elsewhere. For this reason, we want to study another useful parameter that is the effective attenuation.

The effective attenuation (EA) is defined as the difference between the height of the first peak of the model without resonators and the average between the height of the two peaks adjacent to the anti-resonance that comes out after the installation of the resonators. In particular, it indicates how much the tuned mass dampers actually attenuate, considering the energy involved over a certain frequency range. Notice that the attenuation of the first peak produces two sided peaks that can give more relevance to other frequencies.

The other interesting parameter we want to study is the bandwidth (BW), that is the frequency range over which the attenuation of the response is detected.

Therefore, we have two specific objectives to achieve.

Our first aim is to find the best values of the mass-spring-dashpot system for the optimal design of the tuned mass dampers.

Another objective is to understand what the minimum number of resonators is in order to obtain a good attenuation response.

To achieve these goals and to get a deeper understanding of the behavior of the tuned mass dampers, we perform a parametric study.

4.3 Parametric Study

In this section, the parametric study is thoroughly explained. It includes three main steps:

- Choice of resonator parameters
- The bare minimum
- More piles

First of all, we study the influence of the mass and the damping in order to choose the resonators parameters.

Secondly, we investigate the most minimalistic case of resonators, so that we look at the influence of the number of resonators and the distance of the metapiles from the output point.

Lastly, the third step allows us to understand what happens with more resonators, studying the influence of the spacing between each pile and the number of piles, to obtain a good attenuation.

4.3.1 Choice of resonator parameters

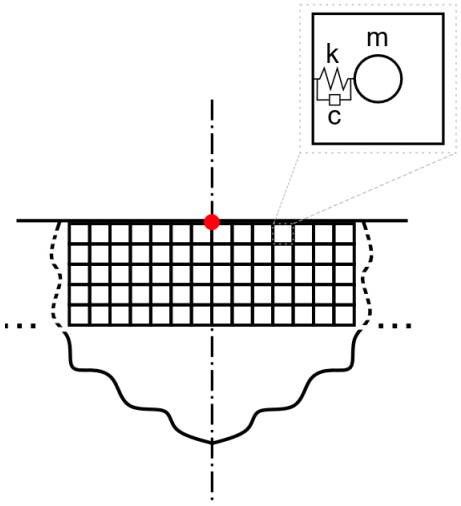

Figure 4. 8: Sketch of the model computed in the first parametric study.

In the first step, we investigate the influence of the mass-spring-dashpot parameters. The schematic in Figure 4.8 shows the model we implement in SAP2000.

In particular, for this specific case, since the influence of the number of resonators here is not important, we assume an ideal case in which the TMDs are widespread everywhere throughout in the half-space.

Notice that this preliminary step is just numerical since it is not feasible in practice, and it would not make sense. In fact, this study step allows us to disengage from other parameters, such as the number of resonators and piles, except for the mass and the damping.

Hence, we choose some values of mass and damping, and we combine them, keeping the natural frequency of the resonator constant at 3.1 Hz.

The masses we analyze are $m\ (t)\ =\ 0.25, 0.5, 1, 1.5, 2, 2.5$, while the values of the viscous damping factor, in percent, are $\xi\ (\%)\ =\ 2, 4, 5, 6, 8, 10, 12, 14, 16$.

Notice that changing the mass and the damping for each distinct model means changing all the parameters of the tuned mass damper so that the resonator remains in resonance conditions.

We know that the resonant frequency at which the resonator is tuned is 3.1 Hz and the period is 0.32 s, reciprocal of the frequency.

The frequency can be defined as:

$$\omega_0 = \sqrt{\frac{k}{m}} = \frac{1}{T}$$

If we want to calculate the stiffness of the tuned mass damper, we can use the following formula:

$$k = \frac{4\pi^2}{T^2} m$$

Another parameter we change in the definition settings of the resonators is the damping constant that depends on the mass, stiffness and damping:

$$C = 2\xi\sqrt{km}$$

By combining all these parameters and creating a distinct model for each combination, we compute all the analyses.

From the results of the steady state analyses, done for each model, and after post-processing the data by means of a MATLAB code, we obtain the transmission response shown in Figure 4.9.

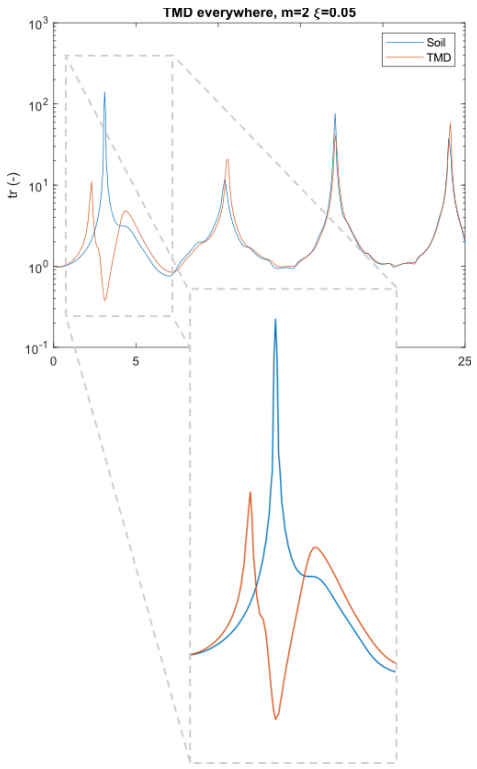

Figure 4. 9: The orange curve shows the transmission response of the model with resonators characterized by a mass of 2 t and a damping of 5 %, while the blue one refers to the model of the soil without resonators.

In particular, this is the superposition of the two transmission curves, where the orange one is obtained for the model with resonators having $m = 2\ t$ and $\xi = 5\ \%$.

In general, all the transmissibility diagrams are similar to the one reported in the picture above, and they allow us to monitor the three parameters: peak attenuation (PA), effective attenuation (EA) and bandwidth (BW).

By post-processing the transmissibility responses with a MATLAB code, we create charts for clearly illustrating the results.

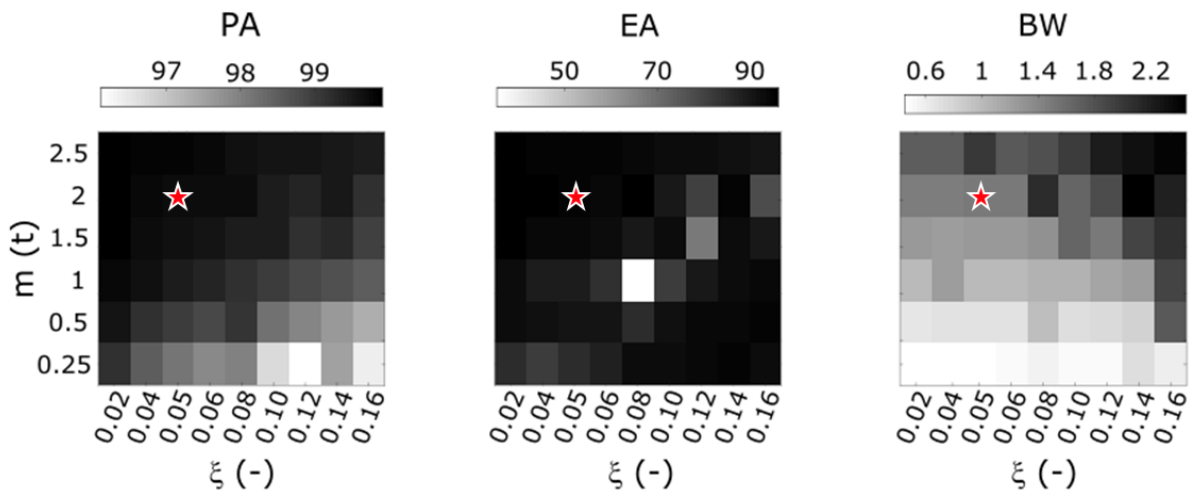

Figure 4. 10: Maps of the peak attenuation, effective attenuation, and bandwidth to study the influence of mass and damping.

The maps in Figure 4.10 show the influence of the mass and the damping, in fact on the y axis there are the values of the mass and on the x axis there are the values of the damping.

The colormap corresponds to a different value of peak attenuation in the first plot, effective attenuation in the second one and bandwidth in the third one.

From the first chart, the more the mass and the less the damping, the higher values are for the peak attenuation, that is ≈ 99 %. Instead, the bandwidth gets worse, but benefits from a high mass and high damping.

We can see that, in this configuration featuring a large number of resonators, even configurations with low masses and high values of damping yield a ≈ 95% attenuation of the peak.

However, the peak attenuation is good for high mass and low damping values. This is not surprising because higher mass means that the resonator has more inertia and, therefore, we can also obtain a better performance. In other words, if we have a soil with many low-mass resonators installed, they can actually resonate but they are not going to give any influence. Hence, the inertia of the resonators needs to be high with the respect to the inertia of the surrounding medium.

Additionally, low damping means that the resonator is more extreme and can undergo larger amplitude, the resonance is going to be more extreme, so we get a bigger difference in between.

From the effective attenuation study, we observe that we do not obtain a clear trend, so it is a bit more challenging to make meaningful considerations. In fact, the graphic shows that for some specific cases the EA value is high, while for others is not so good, i.e. for a damping of 8 %, as reported in Figure 4.11.

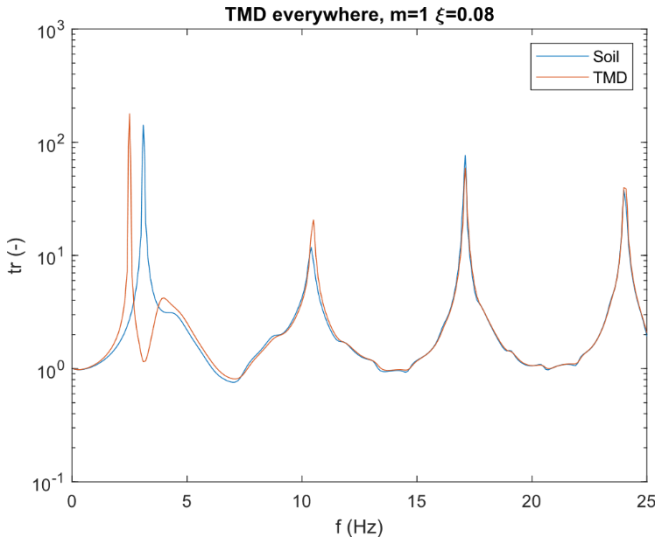

Figure 4. 11: Transmissibility for the bad case with a mass of 1 t and a damping of 8 %.

Considering a mass of 1 t and a damping of 8 %, the effective attenuation is very low. Hence, there are some cases that don't work for us, and it is kind of intuitive because since the response we get is split in two peaks, we have two possibilities: or they are both very high, or one of them is very high with respect to the other one (Figure 4.11). So, it means that even if the peak attenuation is still pretty good, the two-sided peaks are large and give low values of effective attenuation.

As far as the bandwidth is concerned, the reader can notice that things are different and, in particular, the values of bandwidth are good for high mass and for high damping values. This is due to the fact that when the damping is high these peaks are less extreme, they are flatter and therefore they are wider.

In general, we can see that resonators with high mass and low damping or with low mass and high damping behave better than those featuring other combinations of parameters.

Regardless, we need to make a decision and establish which combination of parameters is best for this investigation. What we prioritize in this first study step is not as much the bandwidth, but the signal attenuation. Because of that, we pick a mass of 2 t and a damping of 5%. Moreover, we point out that these properties, together with the overall size of one resonator, are reasonable for realistic design.

4.3.2 The bare minimum

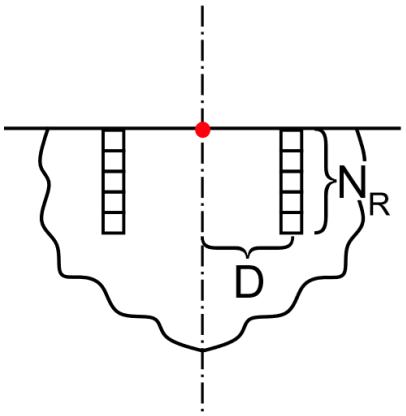

Figure 4. 12: Sketch of the model computed in the second parametric study.

In the second parametric study step, we are eager in looking at the bare minimum, that is the most minimalistic case.

As shown in the schematic in Figure 4.12, instead of considering TMDs everywhere in the half-space, we are interested in reducing the number of resonators to the minimum, examining what

happens if we simulate the half-space with just two piles of resonators. From the previous parametric study, we assume that each resonator has a mass of 2 t and a damping of 5 %.

Therefore, what we study is the influence of the number of resonators of each metapile and the distance between each pile and the control node, that is the midpoint of the upper boundary of the half-space.

The number of resonators we analyze are $N_R = 5, 6, 7, 8, 9, 10$, while the values of the distance are chosen considering the dimensions of a building that we want to isolate. The values of the distance are $D\ (m) = 10, 15, 20, 25, 30$.

We create models combining all these parameters and for each combination, we compute the harmonic analysis to get the transmissibility.

In the following picture (Figure 4.13), the typical transmission response graphic, that we get from the steady state analyses of the model of the soil with only two metapiles, is represented by the orange curve, while the blue one is the response of the reference model. In particular, this is the transmissibility for the case in which we have just two piles of five TMDs each, at a distance from the target point of 10 m.

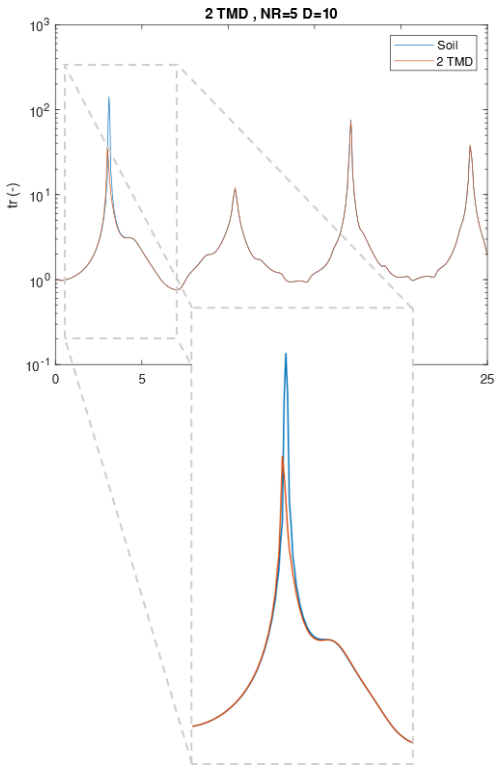

Figure 4. 13: The orange curve shows the transmission response of the model with two piles of five resonators each located at a distance in between of 20 m, while the blue one refers to the model of the soil without resonators.

Also in this case, we focus on the analysis of peak attenuation, effective attenuation and bandwidth, whose trends are described by the colored maps in Figure 4.14.

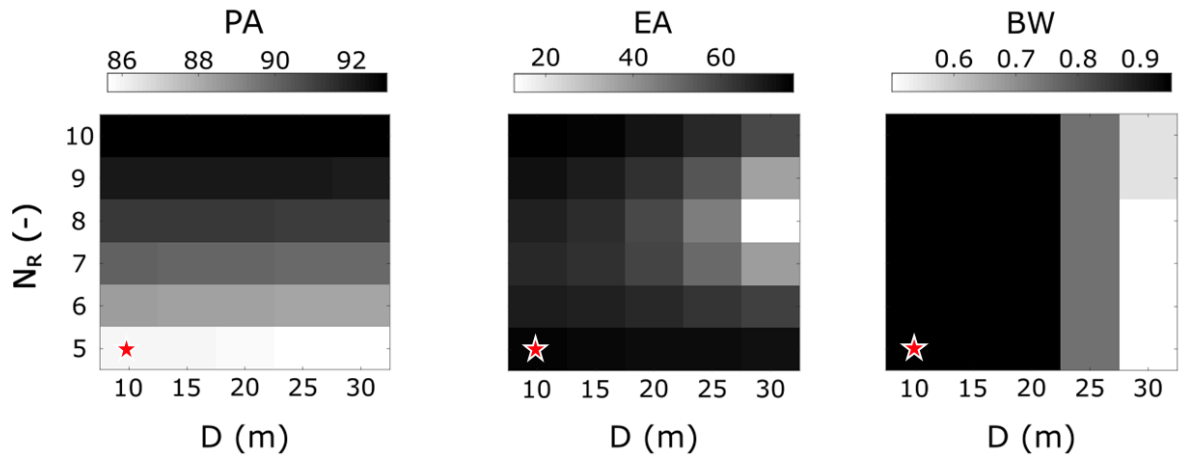

Figure 4. 14: Maps of the peak attenuation, effective attenuation, and bandwidth to study the influence of the number of resonators and the distance between the pile and the center of the half-space.

In these charts, we have on the vertical axis the number of resonators and on the horizontal axis the distance between each metapile and the reference point. The color corresponds to a different value of peak attenuation in the first plot, effective attenuation in the second one and bandwidth in the third one.

The colored map, shown in the first chart, points out that the peak attenuation is high ≈ 92 % if the number of resonators increases, but it is still pretty good ≈ 86 %, if we reduce the number of resonators to five, no matter the distance between them.

This is not surprising since the selected values of D correspond to distances between metapiles between 20 m and 60 m. These values are all smaller than the wavelength in the soil at the frequency of 3.1 Hz, that is 129 m. We know from previous discussions that significant attenuation is expected when the distance between metapiles is smaller than the wavelength of interest.

The trend of the effective attenuation yields less intuitive results, it is pretty good for almost all the combinations, instead it is worse for larger values of distance. In particular, the white point highlights the worst case, that is the one with eight TMDs for each metapile and a distance of 30 m from the reference point. The bandwidth is higher, and close to 1 Hz, if the metapiles are closer to the output point, no matter the number of resonators installed.

For completeness, the worst case for this study step is the one with eight resonators located at a distance from the target location of 30 m. The related transmissibility diagram is reported in Figure 4.15.

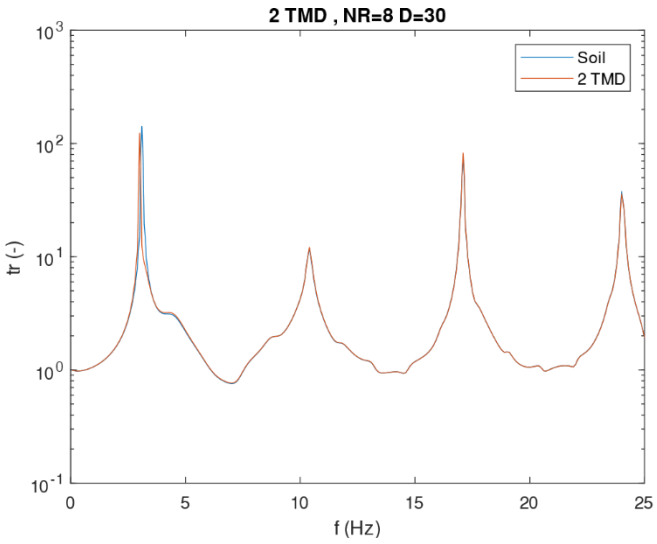

Figure 4. 15: Transmissibility for the bad case with 8 TMDs for each metapile and a distance between them of 60 m.

This study allows us to understand what the minimum number of TMDs we need to install in the half-space is and which the distance in between should be, in order to obtain a satisfactory attenuation.

From this parametric analysis, we understand that if we consider just two piles of five resonators each at a distance from the point of interest of 10 m, there is still a good attenuation.

4.3.3 More piles

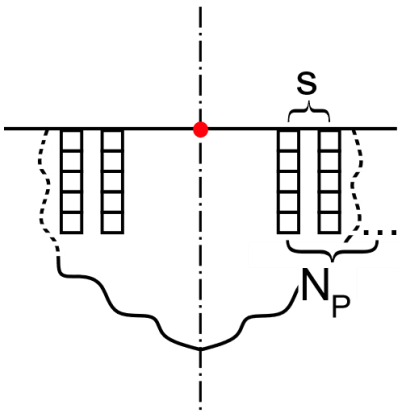

Figure 4. 16: Sketch of the model computed in the third parametric study.

In this section, we move on to the third parametric study step. After validating that a distance of 20 m between the metapiles with five resonators each is suitable for our purpose, we want to study the behavior of more piles. In other words, we consider more metapiles and we vary the spacing between each of them. This idea is depicted in the schematic of Figure 4.16.

Basically, we introduce multiple columns of resonators, so that the values chosen for the number of piles are $N_P = 2, 3, 4, 5$ and they are located at a certain distance between each other, such as $s\ (m) = 2, 4, 6, 8, 10$.

We want to understand the influence of the number of metapiles and their spacing.

In order to study all the combinations of these values, we perform the harmonic analysis for each of them and we obtain the transmission response.

Figure 4.17 illustrates the transmissibility response, in particular we report the case with five metapiles of five resonators each and the spacing between them is 8 m.

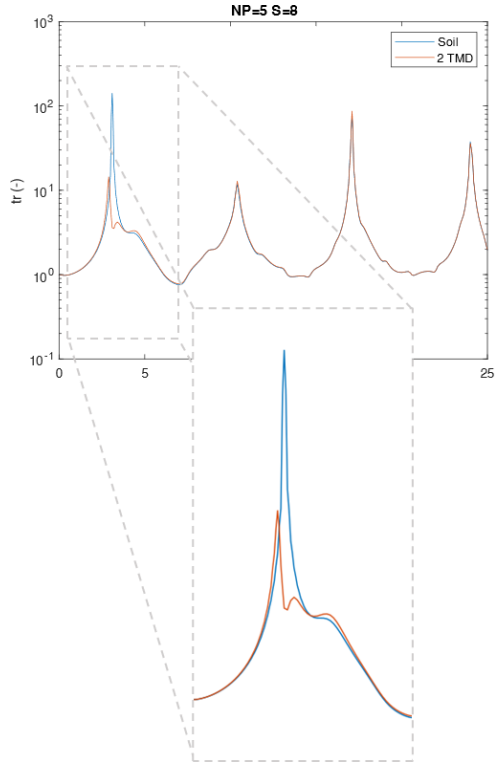

Figure 4. 17: The orange curve shows the transmission response of the model with five piles of five resonators each and the spacing between them is 8 m, while the blue one refers to the model of the soil without resonators.

The transmission curves are post-processed in MATLAB to obtain the colored maps, depicted in Figure 4.18, that allow us to carefully analyze the trend of the peak attenuation, effective attenuation and bandwidth.

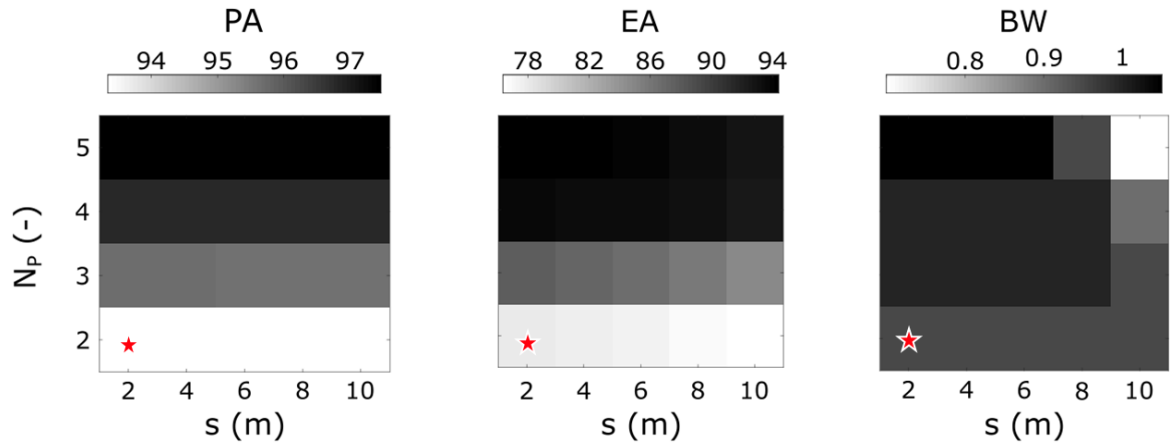

Figure 4. 18: Maps of the peak attenuation, effective attenuation, and bandwidth to study the influence of the number of resonators and the distance between the pile and the center of the half-space.

In these maps, we have the number of metapiles on the vertical axis and the spacing on the horizontal axis. Also in this case, the color corresponds to a different value of peak attenuation in the first plot, effective attenuation in the second one and bandwidth in the third one.

It is clear and intuitive that increasing the number of columns of TMDs, the peak attenuation is higher, no matter what the distance between these columns is. The effective attenuation has exactly the same trend. As for the bandwidth, it is good for all combinations except for five columns spaced 10 m apart. The related bad case is depicted in Figure 4.19.

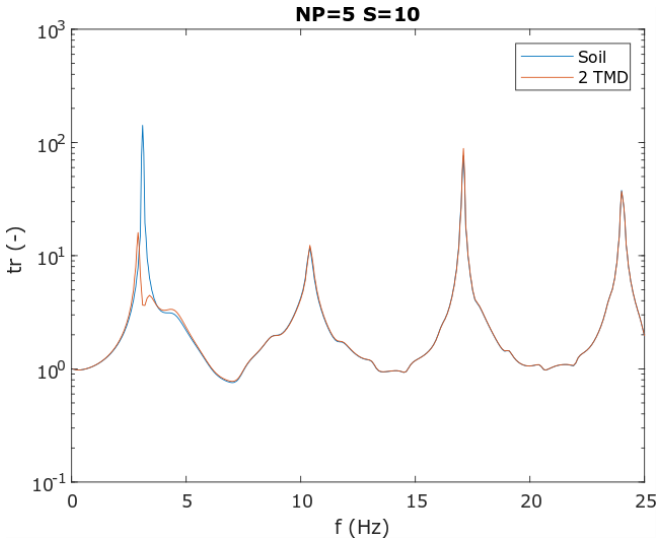

Figure 4. 19: Transmissibility for the bad case with five metapiles where the spacing between them is 10 m.

In light of the previous considerations, we point out that considering just two metapiles the attenuation is ≈ 94 %, that is satisfactory for our purpose.

Additionally, it is really interesting to observe that in the previous charts there is no influence of the distance between metapiles, this is due to the fact that the wavelength is much larger than the distance between the piles. In fact, the wavelength at 3.1 Hz is 129 m, which is much larger than the distances we are talking about. In other words, it does not really matter if we put the metapiles at a distance of 2, 4, 6, 8, 10 m because all these distances are still much smaller than the wavelength. So, that is why there seems not to be much difference, and this is also the reason why in the previous parametric study, the bare minimum, there is no influence of the distance values, because these are still much smaller if compared to the wavelength. Basically, it means that the wavelength is so much larger that cannot go in that space in between.

However, this parametric study represents a powerful tool, in fact depending on the values of the desired wave attenuation and the characteristics of tuned mass dampers, engineers could use these maps to choose how to design the resonator for a specific case. Actually, these maps are very interesting and useful for the engineering community because, by means of these charts, it is possible to make the optimal design and therefore to find the ideal configuration of metapiles.

4.3.4 Using resonators with heterogeneous characteristics

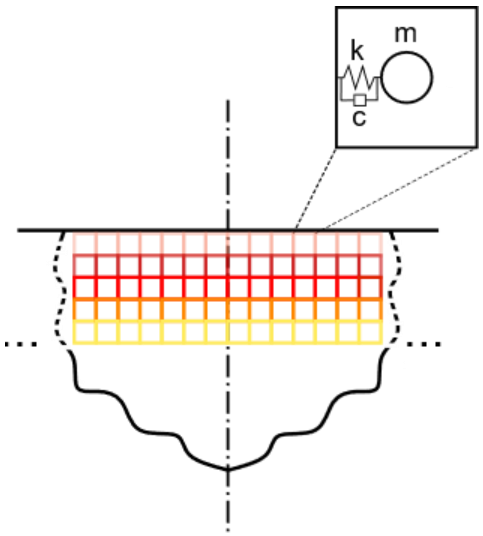

Figure 4. 20: Sketch of the model computed in the random parametric study.

Up until now, our study was carried out with resonators that are all identical to each other, but we are also curious to understand the effects of introducing resonators with slightly different characteristics, varying their spatial arrangements. Essentially, we are interested in looking at the influence of having resonators that can actually resonate at different frequencies. This is in line with the idea of *rainbow trapping*; employing resonators with different characteristics can allow to widen the frequency width of a bandgap [33].

Figure 4.20 explains this idea with colored sketches of resonators, as if the same resonator is located at the same depth below the surface.

Furthermore, we consider a model with TMDs everywhere in the half-space featuring with five resonators for each pile, whose characteristics are a mass of 2 t and a damping of 5%. Then, we select five frequencies at neighboring frequency of 3.1 Hz.

In the following transmissibility diagram, shown in Figure 4.21, the red vertical lines highlight the values of frequency that we choose for the random study. Hence, the frequency values we consider are: $2.5, 2.8, 3.1, 3.4, 3.7\ Hz$.

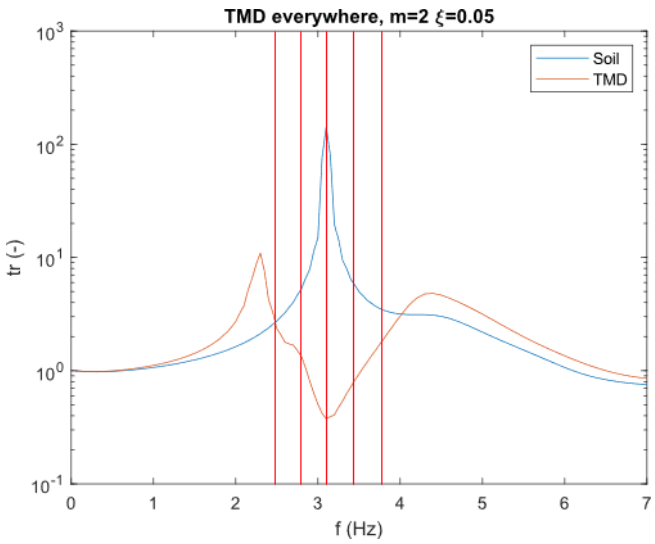

Figure 4. 21: Transmissibility for TMDs everywhere in the half-space, having a mass of 2 t and a damping of 5 %, where the red lines refer to the values of frequencies we choose for this random study.

We arrange resonators with a different frequency of resonance, randomly, creating 20 different combinations and configurations. For instance, COMBO12345 means that resonators of type 1, that has a frequency of resonance of 2.5 Hz is located at the top, immediately below the surface of the soil, the resonator of type 2 with a frequency of resonance of 2.8 Hz, is the second one, then we have the type 3 and 4, hence the type 5 is the last one, at the bottom.

Post-processing the transmissibility diagrams obtained from the harmonic analyses of the models with different spatial arrangement of the resonators, we get the values of peak attenuation, effective attenuation and bandwidth for each combination.

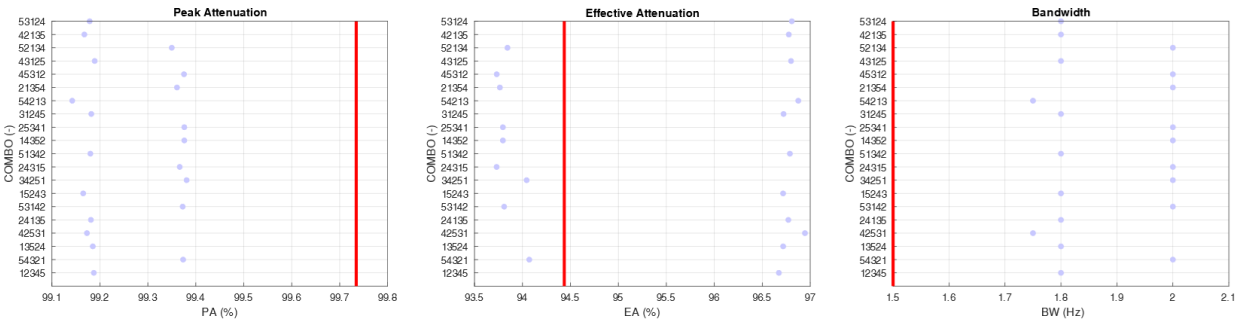

Figure 4. 22: Charts of peak attenuation, effective attenuation and bandwidth for the twenty combinations. The red lines represent the homogeneous case.

In Figure 4.22, the blue markers correspond to the values of the parameters for the heterogeneous cases, where the TMDs that resonate at different frequencies of resonance, are located at different positions in the various models, while the red vertical line highlights the value we obtained for the homogeneous case, where the resonators, tuned at 3.1 Hz, are all identical to each other.

The first chart shows that the peak attenuation is always better for the homogenous case, where the resonators are all identical. Moreover, in the second chart it is possible to notice that in some random cases, in the heterogeneous ones, the effective attenuation is higher than in some homogeneous cases. Instead, the bandwidth is always better for the heterogeneous cases because having resonators of different types allows to spread the wave attenuation regime over multiple frequencies. This is in line with the idea of *rainbow trapping* [33].

4.4 The effects of point-like buildings on the surface of the half-space

Until now, we have studied the wave propagation and attenuation without considering any real structure or building located at the target point of the half-space.

In seismic applications, the design of metafoundations or metabarriers is required when critical infrastructures or sensitive structures, such as hospital or historical buildings, need to be protected from earthquakes and other natural disasters.

In this section, we provide some preliminary results pertaining to a scenario where a simplified structure is located at the target point of the half-space (Figure 4.23).

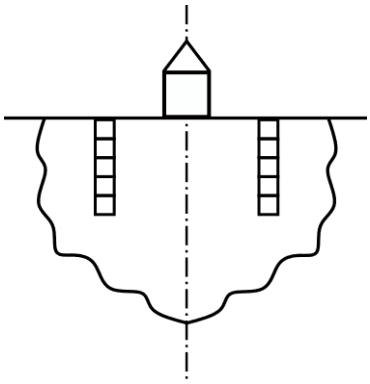

Figure 4. 23: Sketch of the model with two metapiles with five resonators each located at a distance between them of 20 m.

We want to study the most minimalistic case, that is “the bare minimum” previously analyzed in section 4.3.2, in which we consider two metapiles with five resonators each installed underneath the surface at a distance from the target point of 10 m (Figure 4.24).

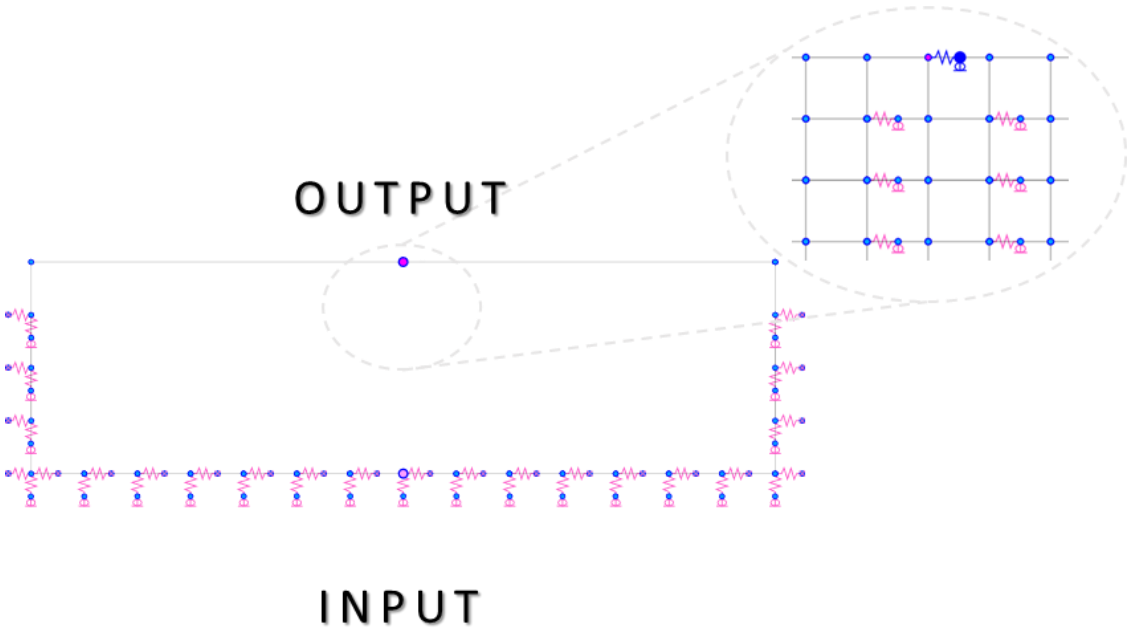

Figure 4. 24: Sketch of the model of the soil with two metapiles and the structure in SAP2000.

Here, we compute the 2D model of the half-space with a structure located at the midpoint of the upper boundary domain. For simplicity, the structure is schematized as a mass-spring-dashpot system, basically a mass connected to a horizontal spring (the blue one), to which we assign the characteristics of stiffness and damping of three floors building elevation.

Note that, in this preliminary study, we consider the building as point-like. Being the depth of the half-space 1 m, we estimate that the 2D structure has a mass of 98 t, consequently the stiffness and the damping coefficient are computed as illustrated in section 4.3.1. Moreover, we also create other two models considering a bit bigger structures, that have respectively twice and thrice the mass of the previous one, 196 t and 294 t. So, in total we have three different models with different structures placed at the target location.

We here assume the structure to have the same resonance as the half-space: 3.1 Hz. This corresponds to a fundamental period of T=0.32 s. Since the structure is schematized as a mass-spring-dashpot system, it also behaves as a tuned mass damper. Thus, we expect the spectrum of the soil response to be attenuated in the presence of the structure.

For each model, we compute a steady state analysis in order to obtain the transmissibility diagram (Figure 4.25). In each of them, the blue curve is relative to the model of the soil plus the structure located at the target point, while the orange one is the transmissibility obtained after the installation of two metapiles in the half-space.

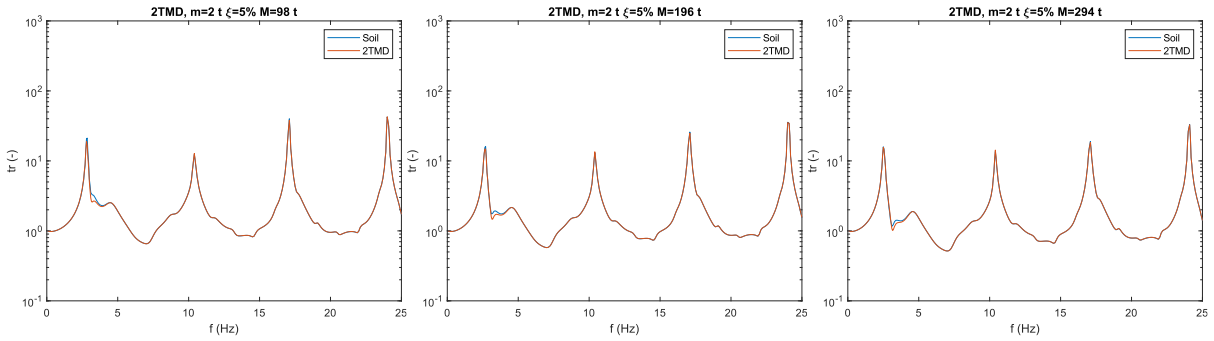

Figure 4. 25: In each graphic, the orange curve shows the transmission response of the model with two piles of five resonators each located at a distance in between of 20 m, while the blue one refers to the model of the soil plus the structure, without resonators.

From the transmission analysis results, we can observe that even if there is a point-like structure in the model, the metapiles still produce an attenuation in the response. In other words, even if the response is largely affected by the presence of the structure, whose large effects are due to its very large inertia, the metapiles still cause some attenuation.

Furthermore, since the mass is applied locally to the target point and given the distance between the output point and the metapiles, there seems to be no dynamic coupling between the superstructure and the resonators within the piles.

Of course, one thing that one should do is an analysis with the structure considering its footprint, not just a schematized building located at a point. In that case, since this structure is going to be closer to the piles, there could be more dynamic coupling.

In fact, other people, like people that have designed metafoundations, where the metamaterials are located immediately underneath the structure, demonstrated that there is a dynamic coupling between the superstructure and the metafoundation [34].

4.5 The effects of earthquake-like accelerogram on wave attenuation

Thus far, our half-space studies have been carried out using steady state excitations. In this section, we want to provide some preliminary results on the effectiveness of this strategy in the presence of earthquake-like excitation accelerogram.

From the National Accelerometric Network website (http://ran.protezionecivile.it/) we download the accelerogram related to a recorded signal whose characteristics are the following: Net Code: IT, Station: TRO, Channel: HNE.

The location is characterized by a Latitude of 40.6145, a Longitude of 16.1422 and an Elevation of 769 m. The reference time of the signal is: 2021:152: 9:11:53.894.

The first sampling is measured at 0 s, the number of measurements is 10527, the sampling interval is 0.005 sps.

The component azimuth is 90 degrees clockwise from Nord, while the component incident angle is 90 degrees from vertical.

The accelerogram of the recorded signal that we choose for this analysis is depicted in Figure 4.26, where there are: (a) the time history of the signal and (b) the Fourier transform of the signal, computed in a MATLAB code.

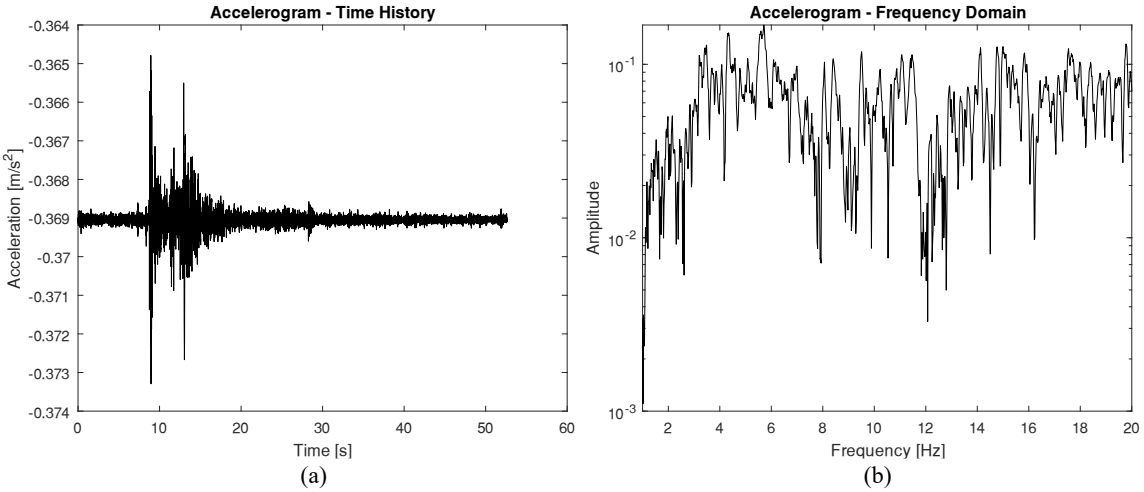

(a) (b)

Figure 4. 26: (a) The time history of the recorded signal of an earthquake. (b) The Fourier transform of the same recorded signal.

This analysis is possible by computing a time history analysis, using the FEM software, SAP2000. We upload the accelerogram in the program and we launch the simulation, from which we obtain the acceleration values recorded at the output point of the half-space, where the structure is located.

By computing these output data in MATLAB, we can build the spectra for the two different models, first for the model without resonators and after for the model with two columns of five resonators each installed below the surface. Figure 4.27 (a) shows the response in the time domain, while Figure 4.27 (b) illustrates the two spectra related to the model without TMDs and the model with the two metapiles installed. In particular, in both charts the blue line is related to the model without metapiles, instead the red line represents the case with two metapiles of five resonators each.

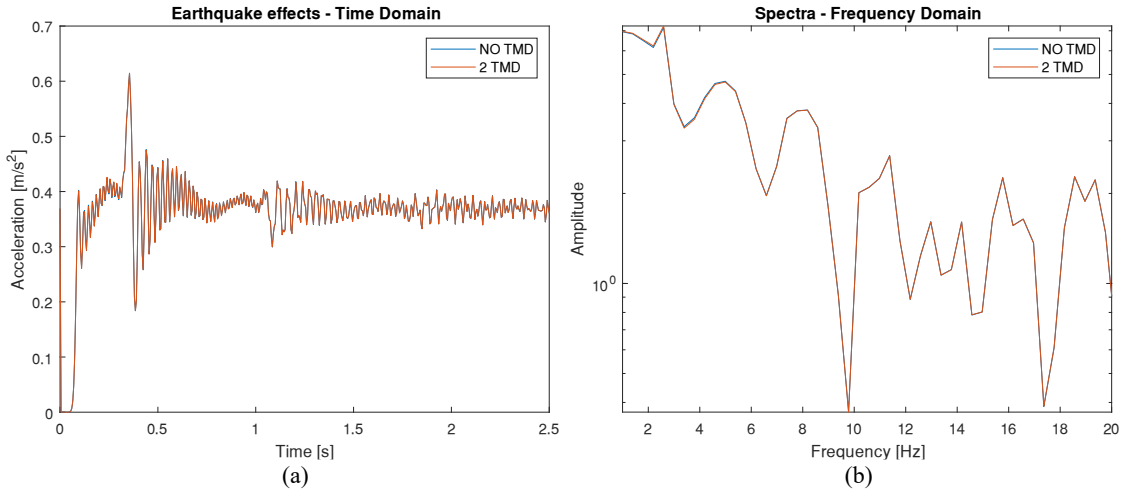

(a) (b)

Figure 4. 27: (a) The response in the time domain. (b) The Fourier transform of the response in the frequency domain.

Since from the first chart (a) it is difficult to clearly understand whether there is attenuation or not, the second graph gives us more information. In fact, by carefully looking at the response in the frequency domain (b), we can see that the presence of metapiles reduces the spectrum around 3 Hz, the frequency at which the resonators are tuned; in fact, one can see that the blue curve, that represents the case without metapiles, is above the orange curve, that refers to the case with two metapiles in the half-space. This reduction of the spectrum confirms that the presence of metapiles allows to obtain wave attenuation.

Notice that the attenuation is more evident in the neighborhood frequency range we are interested in, that is the resonant frequency of the half-space, 3.1 Hz, at which the tuned mass dampers are tuned to resonate.

It must be pointed out that this attenuation is not as significant as the one we register in the steady state analyses discussed in previous sections. This is not surprising, since these metamaterial-based systems are designed to work at specific frequencies and since the earthquake spectrum is very wide-band. Better results could be obtained with more resonators or by using resonators tuned at different frequencies.

4.6 Conclusion

Eventually, we conclude this finite element steady state analysis in SAP2000 considering the semi-infinite medium with soil-like properties and resonators installed below the surface, by pointing out few interesting results.

After this parametric study, we can answer the main question: “What is the minimum number of resonators to obtain a desired attenuation?”. Of course, this depends on the attenuation we intend to obtain.

First of all, we discover that the best resonators parameters are a mass of 2 t and a damping of 5 %. In this specific case we obtain good results, in fact the peak attenuation is very good, about 99%, and the effective attenuation, also a very significant parameter, is about 90% and the bandwidth is 1.5 Hz.

From the second study step we understand that if we consider just two metapiles, the bare minimum number of resonators is five and they are located at a distance of 10 m from the reference point, where is supposed to be the center of the structure that we want to isolate.

Lastly, it is kind of intuitive that the more resonators we put underneath the surface, the greater attenuation we get, but just two metapiles could be enough to obtain a satisfactory effective attenuation. If you have more piles, it improves things but at the same time not dramatically, so it seems like it is not worth it.

The random study is useful for us because validates the fact that the spatial arrangement of different resonators is important. In fact, if one wants to use resonators of different types, a wider frequency attenuation regime may be obtained.

Moreover, we demonstrate that if we consider a building located at the output point of the half-space, we still obtain a reasonable attenuation of the peak by introducing sparse metapiles around the target location to be isolated. Additionally, it is really interesting to highlight that applying a broadband recorded signal of an accelerogram, instead of a harmonic signal, metapiles still show some attenuation capacity at the tuning frequency.

Finally, we conclude that the attenuation provided by metapiles, having specific characteristics and configurations, can be comparable to that provided by metafoundations or huge arrays of resonators located below a target location to be shielded and therefore the employment of metapiles is pretty compelling.

Chapter 5
Conclusion

5.1 Considerations

In this work, we have shown the potential of a new type of metafoundation-like strategy capable of attenuating shear seismic waves propagating in a medium. The project of metapiles constitutes an innovative foundation system, which relies on the concept of locally resonant metamaterials.

First, we demonstrated via numerical simulations that metapiles provide a significant wave attenuation, especially when the distance between the piles is smaller than the wavelength in the medium of interest. When all tuned at the same resonant frequency of 5.9 kHz, our resonators produce a bandgap in which no waves are allowed to propagate [38]. The 3D printed resonators tested with tabletop experimental setup yield promising results validating numerical simulations. The comparison between the data acquired from numerical analyses and experimental results showed a good match, in fact the resonant metamaterials that we designed are capable of attenuating shear seismic wave signals over that specific frequency range, around 6-7 kHz.

Consequently, we wanted to apply the same idea to a different case and investigate what happens if we consider waves propagating in a soil-like properties medium. We implemented a new finite element model, whose results supported and validated previous findings, since we reached the same conclusions.

Furthermore, analyzing different configurations and arrangements of metapiles, we discover that they are capable of achieving an important wave attenuation with only a minimal number of resonators. In particular, the bare minimum corresponds to the installation of two metapiles with five resonators each located at a distance of 20 m between the two columns. From the parametric study, we can affirm that the best combination of resonators parameters is a mass of 2 t and a damping of 5%, that are reasonable for realistic designs.

Metapiles can be installed quite distant from each other and they have potential as noninvasive means for bulk shear wave attenuation.

The promising results of the present research study set the basis for further investigations on the application of composite locally resonant metapiles to redirect and attenuate seismic waves in a specific frequency range.

5.2 Future outlook

There are many questions left to be addressed by future research, involving the interaction between metapiles and the structure to be isolated, since they can have a significant impact on the response of structures subjected to strong earthquakes [34]. It would be necessary to deeply analyze the effects produced by that interaction, in fact the response of the soil influences the motion of the structure and the motion of the structure influences the response of the soil.

Moreover, future work might be directed towards the realization of metapiles with graded characteristics and parameters, to widen the frequency bandwidth of the wave attenuation regime and trying to improve the effective attenuation produced by metapiles [35]. It would be interesting to thoroughly deepen the potential installation of metapiles composed by resonators tuned at different frequencies, around the resonant frequency of the domain.

In order to take into account the feasible structural implementation, it would be very challenging to study the performance of these strategies in real soil media, that are known to hinder some of the wave attenuation effects exhibited by metabarriers [36, 37].

Additional simulations can investigate wider the coupling between metapiles and the structure to be isolated. In fact, the project engineer needs to make sure that the vibration attenuation at a desired frequency does not result in potentially catastrophic vibration amplification at neighboring frequencies [39].

In conclusion, numerical simulations and tabletop experiments make possible the detection of particular phenomena and quantities previously undetected. The application of these metapiles can be valuable to point out many key resonators behavior characteristics related to waveguiding and waves attenuation in a continuous medium.

Appendix – A

Comparison between resonators spring materials

In this appendix, the results obtained for the two strips of different materials are reported.

As previously mentioned, we also use the tabletop experiment as a preliminary step that helps us to determine which material of polyamide is best between the two proposed. So, before choosing the material, we decide to 3D print a series of resonators with the same design (Figure 2.2 (e)), characterized by the four circles around the heavy mass, but made of different materials. Then, we prepare two strips of acrylic, one with the 18 resonators made of white polyamide (PA2200) and the other one with others 18 resonators made of grey polyamide (DM8530), as depicted in picture A.1.

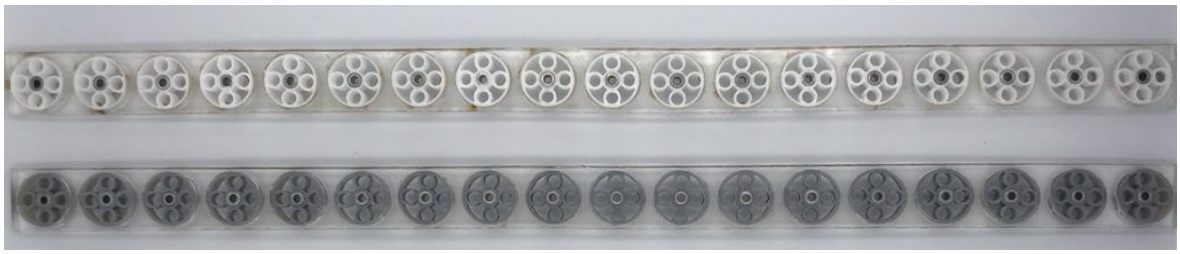

Figure A. 1: Two strips of resonators with different materials. (a) The white resonators are 3D printed with Natural Versatile plastic (PA2200). (b) The grey resonators are 3D printed with Grey 60 (DM8530).

For completeness and to provide a complete view of their behavior, we decide to test them both numerically and experimentally, in order to study the transmissibility response of these two strips. Hence, the results are then elaborated in a MATLAB code, and the transmissibility diagrams are reported in the following pictures.

In Figure A.2, the transmissibility of the strips with the white resonators inserted is illustrated. Hence, the two diagrams show the transmission response, and in particular the black curve refers to the numerical simulation, while the red one refers to the experimental test.

Additionally, looking carefully at these trends, we notice that there is a match between the two bandgaps starting at 5.5 kHz until 7 kHz.

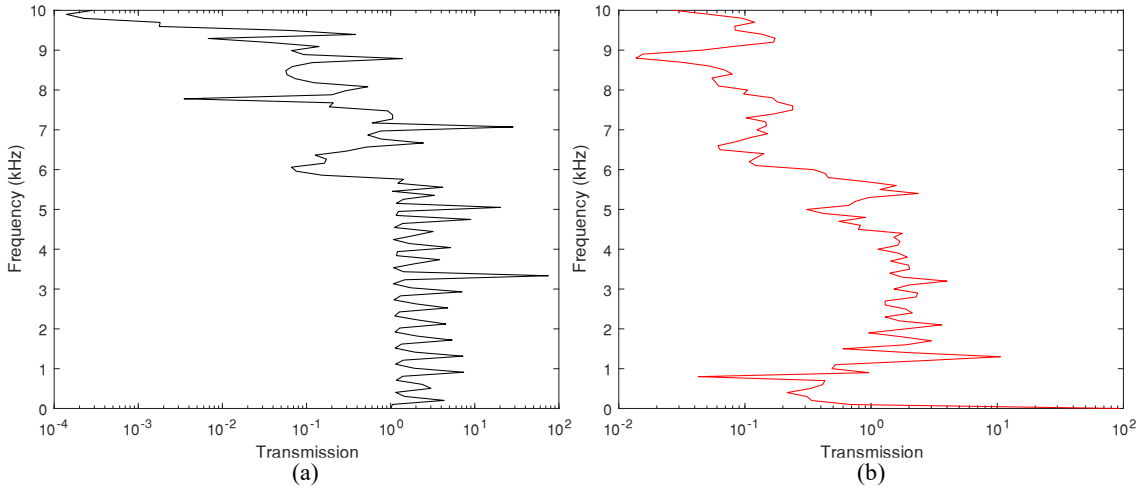

Figure A. 2: (a) The numerical transmissibility for the white resonators. (b) The experimental transmissibility for the white resonators.

The transmissibility of the strips with the grey resonators inserted is shown in Figure A.3. Also in this case, the diagram with the black curve refers to the numerical transmission response, while the red one is obtained by the experimental test.

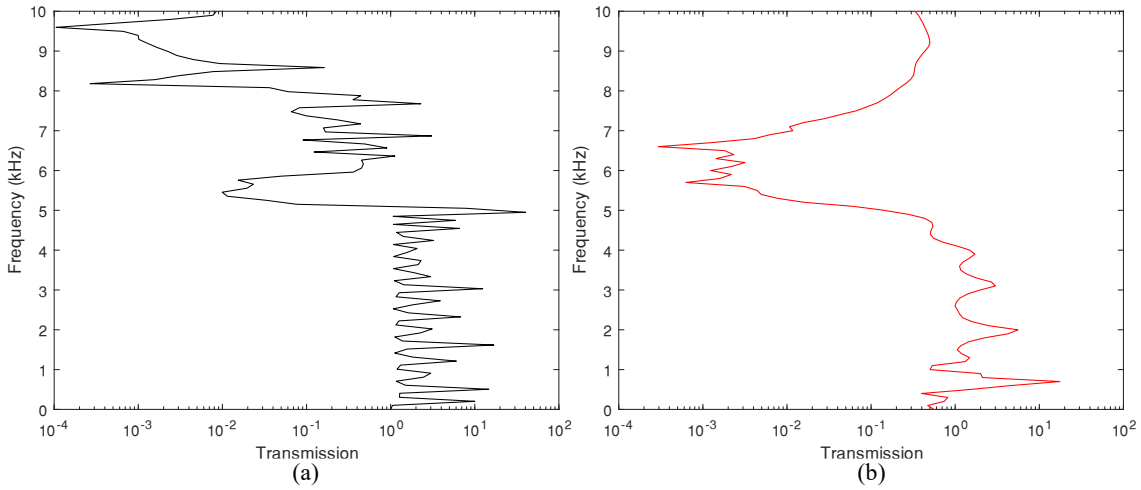

Figure A. 3: (a) The numerical transmissibility for the grey resonators. (b) The experimental transmissibility for the grey resonators.

Both these transmission curves show a bandgap that goes from 5 kHz to 6.3 kHz. In fact, the behavior of the two kinds of resonators is similar and, in both cases, they also match nicely with the bandgap highlighted in the dispersion relations in Figures 2.8 and 2.9 in section 2.2.4.

Since we discover that the difference between the two materials is trivial, we choose to 3D print the resonators with White Natural Versatile Plastic (PA2200) for the following experiments.

Bibliography

[1] M. I. Hussein, M. J. Leamy, M. Ruzzene, Dynamics of phononic materials and structures: Historical origins, recent progress, and future outlook, Applied Mechanics Reviews 66 (4) (2014), doi:10.1115/1.4026911.

[2] W. J. Padilla, D. N. Basov, D. R. Smith, Negative refractive index metamaterials, Science Direct (2006), doi:10.1016/S1369-7021(06)71573-5.

[3] N. Kaina, F. Lemoult, M. Fink, G. Lerosey, Negative refractive index and acoustic superlens from multiple scattering in single negative metamaterials, Nature volume 525, pages77–81 (2015), doi:10.1038/nature14678.

[4] S. Brùlé, E. H. Javelaud, S. Enoch, S. Guenneau, Experiments on seismic metamaterials: Molding surface waves, Physical Review Letters 112 (2014) 133901, doi:10.1103/PhysRevLett.112.133901.

[5] P. Celli, S. Gonella, Manipulating waves with lego bricks: A versatile experimental platform for metamaterial architectures, Applied Physics Letters 107 (8) (2015) 081901, doi:10.1063/1.4929566.

[6] A. Khelif, A. Choujaa, S. Benchabane, B. Djafari-Rouhani, V. Laude, Guiding and bending of acoustic waves in highly confined phononic crystal waveguides, Applied Physics Letters 84 (22) (2004) 4400–4402, doi:10.1063/1.1757642.

[7] M. Oudich, M. B. Assouar, Z. Hou, Propagation of acoustic waves and waveguiding in a two-dimensional locally resonant phononic crystal plate, Applied Physics Letters 97 (19) (2010) 193503, doi:10.1063/1.3513218.

[8] P. Celli, Numerical and experimental characterization of wave processes in phononic crystals, Master Thesis, (2012).

[9] V. La Salandra, M. Wenzel, O. S. Bursi, G. Carta, A. B. Movchan, Conception of a 3D metamaterial-based foundation for static and seismic protection of fuel storage tanks, Frontiers in Materials 4 (2017) 30, doi:10.3389/fmats.2017.00030.

[10] L. Brillouin, Wave propagation in periodic structures, Dover, second edition, 1953.

[11] J. B. Pendry, Negative refraction makes a perfect lens, Journal of Applied Physics (2000), Phys. Rev. Lett. 85, 3966, doi:10.1103/PhysRevLett.85.3966.

[12] R. A. Shelby, D. R. Smith, S. Schultz, Experimental verification of a negative index of refraction, Science (2001) 292(5514):77-9, doi:10.1126/1058847.

[13] Z. Liu, X. Zhang, Y. Mao, Y. Y. Zhu, Z. Yang, C. T. Chan, P. Sheng, Locally resonant sonic materials, Science 289 (5485) (2000) 1734–1736, doi:10.1126/science.289.5485.1734.

[14] N. Stenger, M. Wilhelm, M. Wegener, Experiments on elastic cloaking in thin plates, Journal of Applied Physics (2012), Phys. Rev. Lett. 108, 014301, doi:10.1103/PhysRevLett.108.014301.

[15] L. Zigoneanu, B. Popa, S. A Cummer, Three-dimensional broadband omnidirectional acoustic ground cloak, Nature materials 13, pages352–355 (2014), 10.1038/nmat3901.

[16] C. Sugino, S. Leadenham, M. Ruzzene, On the mechanism of bandgap formation in locally resonant finite elastic metamaterials, Journal of Applied Physics (2016) 120(13):134501, doi:10.1063/1.4963648.

[17] Z. Cheng, Z. Shi, Composite periodic foundation and its application for seismic isolation, Earthquake Engineering & Structural Dynamics 47(4):925-944, doi:10.1002/eqe.2999.

[18] O. Casablanca, G. Ventura, F. Garescì, B. Azzerboni, B. Chiaia, M. Chiappini, G. Finocchio, Seismic isolation of buildings using composite foundations based on metamaterials, Journal of Applied Physics 123 (17) (2018) 174903, doi:10.1063/1.5018005.

[19] A. Colombi, R. Zaccherini, G. Aguzzi, A. Palermo, E. Chatzi, Mitigation of seismic waves: metabarriers and metafoundations bench tested, Journal of Sound and Vibration 485 (2020) 115537, doi:10.1016/j.jsv.2020.115537.

[20] S. J. Mitchell, A. Pandolfi, M. Ortiz, Metaconcrete: designed aggregates to enhance dynamic performance, Journal of the Mechanics and Physics of Solids 65 (2014) 69–81, doi:10.1016/j.jmps.2014.01.003.

[21] D. J. Colquitt, A. Colombi, R. V. Craster, P. Roux, S. R. L. Guenneau, Seismic metasurfaces: Sub-wavelength resonators and Rayleigh wave interaction, Journal of the Mechanics and Physics of Solids 99 (2017) 379–393, doi:10.1016/j.jmps.2016.12.004.

[22] A. Colombi, P. Roux, S. Guenneau, P. Gueguen, R. V. Craster, Forests as natural seismic metamaterials: Rayleigh wave bandgaps induced by local resonances, Scientific Reports 6 (2016) 19238, doi:10.1038/srep19238.

[23] P. Roux; D. Bindi; T. Boxberger; A. Colombi; F. Cotton; I. Douste-Bacque; S. Garambois; P. Gueguen; G. Hillers; D. Hollis; T. Lecocq; I. Pondaven, Toward Seismic Metamaterials: The METAFORET Project, Seismological Research Letters (2018) 89 (2A): 582–593, doi:10.1785/0220170196.

[24] A. Palermo, S. Krödel, A. Marzani, C. Daraio, Engineered metabarrier as shield from seismic surface waves, Scientific Reports 6 (2016) 39356, doi:10.1038/srep39356.

[25] M. V. Barnhart, X. Xu, Y. Chen, S. Zhang, J. Song, G. Huang, Experimental demonstration of a dissipative multi-resonator metamaterial for broadband elastic wave attenuation, Journal of Sound and Vibration 438 (2019) 1–12, doi:10.1016/j.jsv.2018.08.035.

[26] Ricker, N. The form and laws of propagation of seismic wavelets, Geophysics 18, 10-40 (1953).

[27] Y. Wang, Frequencies of the Ricker wavelet, Geophysics 80 (2) A31-A37 (2015) doi:10.1190/geo2014-0441.1.

[28] A. Amorosi, D. Boldini, Numerical modelling of the transverse dynamic behaviour of circular tunnels in clayey soils, Soil Dynamics and Earthquake Engineering 29 (6) (2009) 1059–1072, doi:10.1016/j.soildyn.2008.12.004.

[29] J. Wang, W. Sun, S. Anand, Numerical investigation on active isolation of ground shock by soft porous layers, Journal of Sound and Vibration 321 (3-5) (2009) 492–509, doi:10.1016/j.jsv.2008.09.047.11.

[30] P. A. Vermeer, R. B. J. Brinkgreve, Plaxis finite element code for soil and rock analyses, Balkema, Rotterdam-Brookfield, Netherlands (1998) 1–114.

[31] J. Lysmer, R. L. Kuhlemeyer, Finite dynamic model for infinite media, Journal of the Engineering Mechanics Division 95 (4) (1969) 859–878, doi:10.1061/JMCEA3.0001144.

[32] S. L. Kramer, Geotechnical earthquake engineering, Pearson Education India, 1996.

[33] S. Krödel, N. Thomé, C. Daraio, Wide band-gap seismic metastructures, Extreme Mechanics Letters 4 (2015) 111–117, doi:10.1016/j.eml.2015.05.004.

[34] L. Xiao, F. Sun, O. S. Bursi, Vibration attenuation and amplification of one-dimensional uncoupled and coupled systems with optimal metafoundations, Journal of Engineering Mechanics 146 (7) (2020) 04020058, doi:10.1061/(ASCE)EM.1943-7889.0001786.

[35] K. H. Matlack, A. Bauhofer, S. Krödel, A. Palermo, C. Daraio, Composite 3d-printed metastructures for low-frequency and broadband vibration absorption, Proceedings of the National Academy of Sciences 113 (30) (2016) 8386–8390, doi:10.1073/pnas.1600171113.

[36] A. Palermo, S. Krödel, K. H. Matlack, R. Zaccherini, V. K. Dertimanis, E. N. Chatzi, A. Marzani, C. Daraio, Hybridization of guided surface acoustic modes in unconsolidated granular media by a resonant metasurface, Physical Review Applied 9 (2018) 054026, doi:10.1103/PhysRevApplied.9.054026.

[37] R. Zaccherini, A. Colombi, A. Palermo, V. K. Dertimanis, A. Marzani, H. R. Thomsen, B. Stojadinovic, E. N. Chatzi, Locally resonant metasurfaces for shear waves in granular media, Physical Review Applied 13 (2020) 034055, doi:10.1103/PhysRevApplied.13.034055.

[38] H. H. Huang, C. T. Sun, G. L. Huang, On the negative effective mass density in acoustic metamaterials, International Journal of Engineering Science 47 (4) (2009) 610–617, doi:10.1016/j.ijengsci.2008.12.007.

[39] F. Sun, L. Xiao, O. S. Bursi, Quantification of seismic mitigation performance of periodic foundations with soil-structure interaction, Soil Dynamics and Earthquake Engineering 132 (2020) 106089, doi:10.1016/j.soildyn.2020.106089.

[40] V. K. Dertimanis, I. A. Antoniadis, E. N. Chatzi, Feasibility analysis on the attenuation of strong ground motions using finite periodic lattices of mass-in-mass barriers, Journal of Engineering Mechanics 142 (9) (2016) 04016060, doi:10.1061/(ASCE)EM.1943-7889.0001120.

[41] L. Burrows, A toolkit for transformable materials: how to design materials with reprogrammable shape and function (2017).

[42] A. Colombi, D. J. Colquitt, P. Roux, S. Guenneau, R. V. Craster, A seismic metamaterial: The resonant metawedge, Scientific Reports 6 (1) (2016) 1–6, doi:10.1038/srep27717.

[43] M. Miniaci, A. Krushynska, F. Bosia, N. M. Pugno, Large scale mechanical metamaterials as seismic shields, New Journal of Physics 18 (8) (2016) 083041, doi:10.1088/1367-2630/18/8/083041.

[44] Muhammad, C. W. Lim, J. N. Reddy, Built-up structural steel sections as seismic metamaterials for surface wave attenuation with low frequency wide bandgap in layered soil medium, Engineering Structures 188 (2019) 440–451, doi:10.1016/j.engstruct.2019.03.046.

[45] F. Basone, M. Wenzel, O. S. Bursi, M. Fossetti, Finite locally resonant metafoundations for the seismic protection of fuel storage tanks, Earthquake Engineering & Structural Dynamics 48 (2) (2019) 232–252, doi:10.1002/eqe.3134.

[46] SAP2000, Inc., SAP2000 Theory manual, Version 20.

[47] COMSOL Multiphysics, Inc., COMSOL Theory manual, Version 5.4, 2018.